EPRI | ELECTRIC POWER RESEARCH INSTITUTE

Evaluation of Partial Discharge (PD) Testing Technology for Transmission Class Cables

1012338

Evaluation of Partial Discharge (PD) Testing Technology for Transmission Class Cables

1012338

Technical Update, December 2006

EPRI Project Manager

S. Eckroad

ELECTRIC POWER RESEARCH INSTITUTE
3420 Hillview Avenue, Palo Alto, California 94304-1338 ▪ PO Box 10412, Palo Alto, California 94303-0813 ▪ USA
800.313.3774 ▪ 650.855.2121 ▪ askepri@epri.com ▪ www.epri.com

DISCLAIMER OF WARRANTIES AND LIMITATION OF LIABILITIES

THIS DOCUMENT WAS PREPARED BY THE ORGANIZATION(S) NAMED BELOW AS AN ACCOUNT OF WORK SPONSORED OR COSPONSORED BY THE ELECTRIC POWER RESEARCH INSTITUTE, INC. (EPRI). NEITHER EPRI, ANY MEMBER OF EPRI, ANY COSPONSOR, THE ORGANIZATION(S) BELOW, NOR ANY PERSON ACTING ON BEHALF OF ANY OF THEM:

(A) MAKES ANY WARRANTY OR REPRESENTATION WHATSOEVER, EXPRESS OR IMPLIED, (I) WITH RESPECT TO THE USE OF ANY INFORMATION, APPARATUS, METHOD, PROCESS, OR SIMILAR ITEM DISCLOSED IN THIS DOCUMENT, INCLUDING MERCHANTABILITY AND FITNESS FOR A PARTICULAR PURPOSE, OR (II) THAT SUCH USE DOES NOT INFRINGE ON OR INTERFERE WITH PRIVATELY OWNED RIGHTS, INCLUDING ANY PARTY'S INTELLECTUAL PROPERTY, OR (III) THAT THIS DOCUMENT IS SUITABLE TO ANY PARTICULAR USER'S CIRCUMSTANCE; OR

(B) ASSUMES RESPONSIBILITY FOR ANY DAMAGES OR OTHER LIABILITY WHATSOEVER (INCLUDING ANY CONSEQUENTIAL DAMAGES, EVEN IF EPRI OR ANY EPRI REPRESENTATIVE HAS BEEN ADVISED OF THE POSSIBILITY OF SUCH DAMAGES) RESULTING FROM YOUR SELECTION OR USE OF THIS DOCUMENT OR ANY INFORMATION, APPARATUS, METHOD, PROCESS, OR SIMILAR ITEM DISCLOSED IN THIS DOCUMENT.

ORGANIZATION(S) THAT PREPARED THIS DOCUMENT

Electrical Insulation Research Center

This is an EPRI Technical Update report. A Technical Update report is intended as an informal report of continuing research, a meeting, or a topical study. It is not a final EPRI technical report.

NOTE

For further information about EPRI, call the EPRI Customer Assistance Center at 800.313.3774 or e-mail askepri@epri.com.

Electric Power Research Institute and EPRI are registered service marks of the Electric Power Research Institute, Inc.

CITATIONS

This document was prepared by

Electrical Insulation Research Center
Institute of Materials Science
University of Connecticut
97 North Eagleville Road
Storrs, CT 06269-23136

Principal Investigators
S. Boggs
C. Xu
L. Zhang

This document describes research sponsored by the Electric Power Research Institute (EPRI).

This publication is a corporate document that should be cited in the literature in the following manner:

Evaluation of Partial Discharge (PD) Testing Technology for Transmission Class Cables. EPRI, Palo Alto, CA: 2006. 1012338.

ABSTRACT

The objective of this project is to evaluate options for field partial discharge (PD) testing of transmission class solid dielectric cable, both laminar and solid dielectric. This report presents an introduction into partial discharge testing followed by a mathematical development of partial discharge pulse propagation in shielded power cable which can be used as a basis for predicting PD detection sensitivity. The theory covers both narrow Gaussian PD pulses and broader, asymmetric pulses.

A critical literature review summarizes the approaches which have been published for PD detection in transmission class solid dielectric cable. Several approaches have achieved a PD detection sensitivity of better than 10 pC over an entire cable installation and a sensitivity of about 1 pC near the PD couplers, which are usually located at splices although not necessarily at every splice.

As the literature review revealed little related to PD detection or high frequency loss in laminar dielectric cable, samples of unimpregnated and impregnated 345 kV PPLP HPFF cable were obtained from The Okonite Company. The detailed structure of the cable was analyzed and high frequency dielectric properties of the PPLP dielectric and carbon impregnated paper semiconducting layers were measured. The high frequency loss of the cable was predicted on the bases of this information; however, the complex ground structure of the cable makes the loss in the ground conductors uncertain. As a result, measurements of high frequency cable loss of impregnated 345 kV PPLP cable were undertaken at the Okonite factory in Paterson, NJ. The conclusion of these measurements and the analysis is that the complex ground structure of PPLP cable results in large high frequency loss which will make PD measurement difficult.

The literature also revealed little data related to the high frequency loss of transmission class solid dielectric cable, which differs appreciably from distribution cable in the inclusion of "bedding layers". As a result, high frequency attenuation measurements for two constructions of transmission class solid dielectric cable were carried out at the Southwire facility in Oxford, AL.

The high frequency loss of the PPLP cable is substantially greater than that of the XLPE cables. In the case of the transmission class XLPE cable measured, the loss constant increases more or less linearly with frequency to a "turnover" frequency, above which the loss becomes constant. This turnover frequency ranges from 10 MHz to 18 MHz and is the result of the high resistivity of the bedding. This "turnover" is not typical of solid dielectric distribution cable, which lacks bedding layers.

Based on the measured properties of PPLP and transmission class solid dielectric cable, PD monitoring appears to be more realistic for the latter than for the former. The application of state of the art high resolution (12 to 14 bit) high speed (250 to 150 MHz) A/D converters, combined with the large available high speed memory, state-of-the-art digital signal processing (e.g., wavelet analysis), and recently developed algorithms which allow PD pulses from multiple PD sources to be clustered and analyzed separately should open the way to a practical on-line PD monitoring system for transmission class solid dielectric cable.

ACKNOWLEDGEMENTS

The authors are pleased to acknowledge The Okonite Company and Forte Power Systems, a subsidiary of the Southwire Company, for access to and help during measurements of the high frequency loss of transmission class cables at their facilities in Patterson, NJ and Oxford, AL, respectively.

CONTENTS

1
INTRODUCTION

How Does a Small Defect Cause Failure of a Large Gap

This is the most fundamental question in the field of electrical insulation degradation and failure. The mechanisms for gaseous and solid dielectrics are similar but with time scales which differ by orders of magnitude and are probably related to the viscosity.

Gaseous Dielectrics

The world is not symmetric with respect to positive and negative carriers, i.e. negative carriers are usually electrons, which are very light, while positive carriers are usually ions, which are much heavier. As a result, positive and negative breakdown are not symmetric. We will describe the case of highly inhomogeneous field breakdown from the negative electrode of an electronegative dielectric gas, such as SF_6 [1], i.e., where we have a relatively small defect which raises the field above the breakdown field of the gas in a region which is small compared to the overall dielectric gap. In this case, breakdown starts with corona (streamer formation) around the defect tip. The corona extends to a distance at which the electric field falls below that of the breakdown field of the gas, and the field in this streamer filled region is generally about the breakdown field of the gas. Once this high field region fills with space charge, nothing much more can happen immediately, so all visible (discharge) activity stops for some 10's of ns. However the electrons and negative ions drift away from the negative stress enhancement, and the positive ions drift toward the stress enhancement. This implies a charge separation at the edge of the streamer region, and charge separation raises the electric field. But the electric field at that boundary was already at the breakdown field of the gas, so any increase raises the electric field above the breakdown field. Thus light emission starts to occur from this boundary region, and eventually (ns) a breakdown occurs from the boundary region back to the tip of the stress enhancement. This breakdown forms a leader, which is a high conductivity, high temperature gas channel, which then acts as a stress enhancement sticking out into the gas, and the process repeats from the tip of that stress enhancement. Thus breakdown across the entire gap occurs in a stepwise manner which repeats the above process. Thus a small stress enhancement can cause failure of the entire gap because the breakdown process creates its own stress enhancement as it goes along, and breakdown occurs in a stepwise manner which can take microseconds to complete the path across the gas gap. The details of the process differ somewhat for positive and negative breakdown, and for electronegative (O_2, SF_6, etc.) and nonattaching gases (N_2, etc.), so the details of the above process should not be taken as universal. However, the idea of the breakdown channel creating its own stress enhancement which promotes further breakdown is universal.

Solid Dlelectrics

The situation in solid dielectrics is very similar to that in gaseous dielectrics. In the case of a pre-existing cavity, discharge within the cavity tends to cause roughening of the cavity surface.

If the cavity surface is easily carbonized or converted to a semiconducting state, the cavity may cease to discharge. More likely, the continued roughening of the cavity surface will result in a discharge tubule growing out of the cavity in the general direction of the electric field. This tubule will form branches like a lightning strike, and discharges will occur down the tubule branches. These discharges tend to make the tubule surfaces conducting which enhances the electric field at the tips of the tubules. The exact process by which the tubules grow is not known. However the partial discharge magnitudes tends to be small when the tubules are growing rapidly and large when they are not. This suggests that the tubules grow by a high field electromechanical mechanism which causes weakening of the dielectric as a result of charge injection, hot electrons, and UV photon generation [2] followed by yielding of the weakened dielectric as a result of cyclic electromechanical forces associated with the AC electric field acting on the injected charge [3]. Once the channel has grown to a point that too large a voltage drop occurs across the channel walls, rapid growth stops, and discharge occurs in the channel until the channel walls become sufficiently conductive to the channel tip, after which growth resumes. While the above growth process is "logical", it is not established fact. In any case, once such a dendritic pattern ("electrical tree") starts, it usually grows to completion, unless the dielectric contains barriers which "disperse" the injected charge, such as mica, which has a much greater in-plane conductivity than through plane conductivity.

In the case of a stress enhancement on an electrode or caused by a conducting contaminant, an electrical tree will be initiated if the field at the tip of the conducting stress enhancement is greater than the space charge limited field, i.e., the field for high carrier mobility. Again, electrical trees tend to be harder to initiate than to grow, so once they are initiated, they usually grow to failure. In the case of a conducting stress enhancement, the process starts with charge injection from the tip of the stress enhancement and cycling of the charge in and out of the tip as a result of the AC field. This causes the positive and negative carriers to "pass through" each other, which results in carrier recombination, UV photon emission which can break chemical bonds, etc. Degradation of the dielectric in the region of the stress enhancement creates a cavity which can support partial discharge, and an electrical tree is initiated from the cavity. During the tree initiation phase, which involves only charge injection, no measurable electrical signal is present. An electrical signal can be measured under very specific laboratory conditions, but certainly not under normal field conditions. The first "discharges" which occur are likely to be in the range of 0.1 pC, also too small to be detected under most field conditions. The time required to initiate an electrical tree which generates partial discharge signals of 10 pC or greater can be many hours, days, or even years. Thus such stress enhancements may not be detected during a factory test but may cause failure in service. This is one of the reasons why quality cannot be "tested into" dielectric systems, as defects can occur which will not be detected during any practical factory test but which will cause failure in service.

Thus for solids, as for gases, the mechanism by which a small but severe defect causes failure of the entire dielectric gap involves a step-wise mechanism through which the breakdown mechanism creates its own stress enhancement which allows the breakdown to progress, in a stepwise manner, across the entire gap. The fact that the steps progress much more slowly in a solid than in a gas offers the possibility of using discharge phenomena during growth, usually called "partial discharge", as a diagnostic.

References

1. Wiegart, N., L. Niemeyer, F. Pinnekamp, W. Boeck, J. Kindersberger, R. Morrow, W. Zaengl, M. Zwicky, I. Gallimberti, and S.A. Boggs. "Inhomogeneous Field Breakdown in GIS - The Prediction of Breakdown Probabilities and Voltages. Part I: Overview of a Theory for Inhomogeneous Field Breakdown in SF6. IEEE Trans. Power Delivery, Vol. 3, July, 1988, p. 923.
2. Cao, Yang and S.A. Boggs. "Mechanisms of High Field Electroluminescence and Detemrination of the Space Charge Limited Field in Polymeric Dielectrics". IEEE Trans. PD-12, No. 4, August 2005. pp. 690-699.
3. Boggs, S.A. "Very High Field Phenomena in Dielectrics". IEEE Trans DEI-12, Oct. 2005, pp. 929-938.

2

PARTIAL DISCHARGE PULSE PROPAGATION AND DETECTION IN CABLES

Introduction

The measured partial discharge signal results from the change in image charge on the electrodes of a system when a discharge takes place within the system. Figure 1 shows the example of discharge within a cavity between two electrodes. The discharge causes the field within the cavity to fall to near zero within ns. This is equivalent to filling the cavity with a conducting solid, which would increase the capacitance between the electrodes. Since charge cannot normally transfer to the electrodes on the nanosecond scale of the discharge, the voltage on the electrode drops on a transient basis. In the PD detection scheme shown in Figure 1, the PD signal generated across the coupling unit is caused by the current which charges the increased sample capacitance after the discharge. As seen in Figure 1, the field in the cavity after the discharge is very small as a result of ions drifting to the walls of the cavity in a pattern which tends to cancel the field within the cavity (Figure 2). The current in the cavity consists of a fast, high current electronic part and a much slower ionic (Figure 3). The high mass of the ions relative to the electrons causes the ionic mobility to be orders of magnitude less than the electronic mobility. As a result, only the electronic portion of the signal is normally observed. When great care is taken to measure the partial discharge waveform with a wide bandwidth, we can see that the voltage in the cavity collapses in one to several nanoseconds (Figure 4).

PD Inception vs Extinction Voltage

Figure 5 shows an idealized PD pattern for cavity discharge. Note that the discharges tend to collect around the voltage zero, where dV/dt is maximum. As seen from Figure 2, the cavity starts with no charge before the first partial discharge. Thus to obtain the first discharge, the voltage must be raised to the point that the field in the cavity is above the breakdown field. After the first discharge, which is likely to occur near the peak applied voltage, the field in the cavity is near zero, i.e., the field in the cavity is near zero at (near) the peak applied voltage. Thus when the voltage reverses to the opposite peak, the field in the cavity will be near twice the value which caused the initial breakdown. This is the reason that the PD inception voltage is substantially greater than the PD extinction voltage, because the first discharge must take place without any “biasing” of the field in the cavity by previous discharges. Thus, in theory, the PD initiation voltage can be twice the extinction voltage, while in practice it is typically 1.5 to 1.7 times the extinction voltage.

One implication of the PD inception vs extinction voltage is that an off-line test must be carried out to at least 2 pu in order to “assure” that all PD sources which might be in discharge at normal operating voltage are active during the test. However if the system has been in service for a substantial period of time, then any sources which could be initiated at normal operating voltage

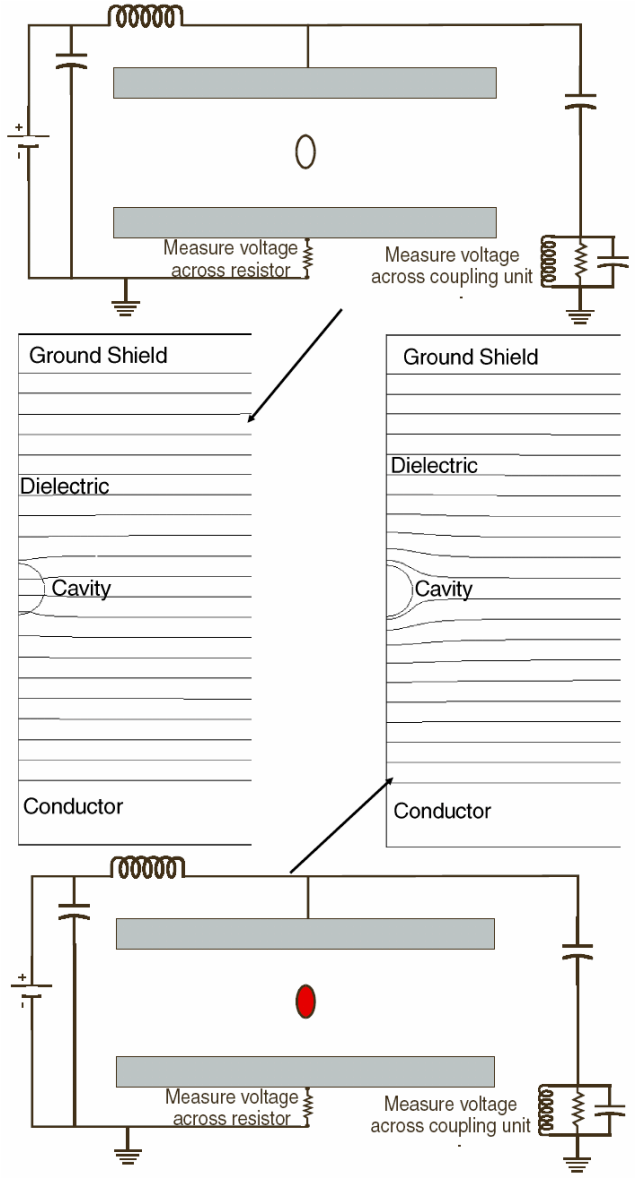

Figure 1 System with cavity (above) and electric field distribution (middle left) prior to a partial discharge. The field in the cavity is higher than that in the solid as a result of the lower dielectric constant of the gas in the cavity. After the discharge (bottom), the field in the cavity is near zero as the discharge "shorts out" the cavity, and ions drift to the walls creating a charge distribution which makes the field in the cavity immediately after the discharge very low.

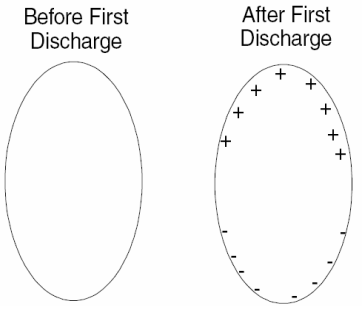

Figure 2. Prior to the first discharge little charge resides in the cavity. After the first discharge, ions move in the electric field to the walls of the cavity in a pattern which tends to cancel the electric field in the cavity. This changes the electric field distribution in the cavity to roughly that which would occur if the cavity were filled with a conductor. The result is an increase in the charge on the electrodes as a result of the increased "capacitance", although this increase could only be measured with a conventional capacitance measurement during the discharge.

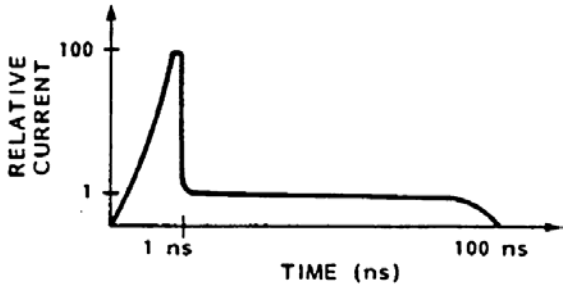

Figure 3. Idealized PD current. The initial, large current is caused by the higher mobility of electrons, while the long tail is caused by the slower ions.

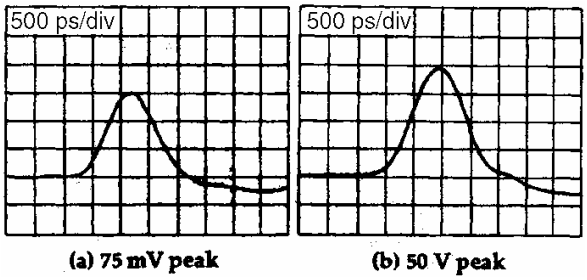

Figure 4. Oscilloscope traces of PD pulses measured in a transmission line geometry with a 1 GHz bandwidth. The smaller signal is generated by particles bouncing in an SF6 gas insulated transmission line (GITL), while the large signal is generated by a floating component in a GITL. The waveforms are very similar, with a risetime near 1 nse, but the amplitudes differ greatly. Only the electronic component of the signal is observed. The 75 mV signal propagatng in a 60 W transmission line corresponds to about 1.25 pC. As can be seen, this small PD signal is detected with good S/N using ultrawideband PD detection.

have probably been initiated by surges, etc. on the system. Thus an in-service test at normal operating voltage is roughly equivalent to an off-line test at 2 pu.

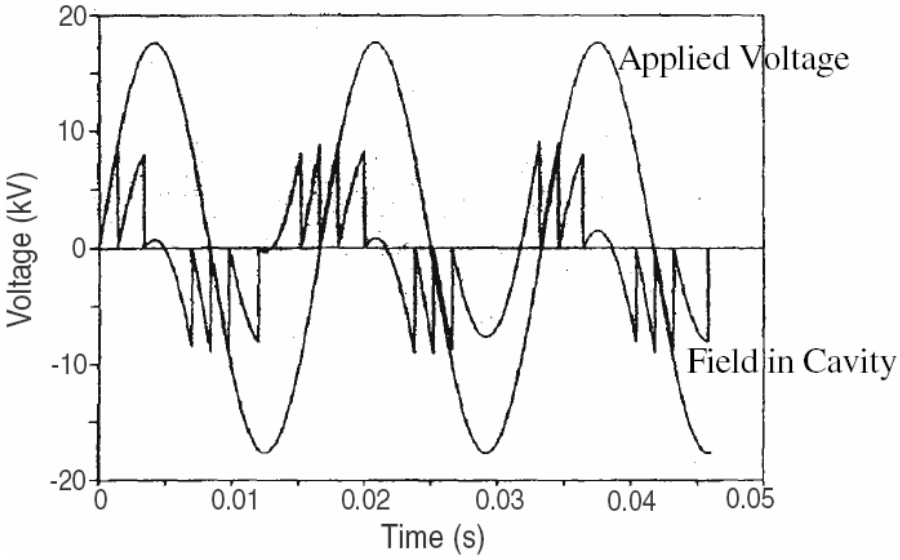

Figure 5. Applied voltage and the electric field within the cavity which results from successive discharges within the cavity. Note that for cavity discharge, the PD pulses tend to collect around the zero crossings of the voltage where the dV/dt is maximum.

Even if the field within a cavity is above the breakdown field of the gas in the cavity, PD will not initiate without an initial electron. For a cavity bounded by dielectrics, the primary source of such electrons is cosmic rays, which generate electrons in air at a rate of about 3 electrons/cm^3-s. For a 1 mm^3 cavity, the average waiting time for an initial electron would be in the range of 5 minutes. Thus even if a cavity is large enough to generate detectable PD and the applied voltage is sufficient to initiate PD, PD may not occur during the test. Under laboratory conditions, use of a small flux of ionizing radiation, e.g., x-rays, increases PD detection sensitivity substantially.

Again, in-service PD detection has the advantage that if self-sustaining PD can be initiated within a cavity, the system has probably been energized for a sufficient time that PD will have been initiated, whereas this may not be true of an off-line test.

PD Signal Characteristics

For almost all systems in which PD is generated, the PD pulse originates with a duration of at most a few nanoseconds (10^{-9} s) and often only one or two ns. However, the signal which is detectable outside the object depends on the nature of the connection between the point of generation and the external world. Under the best conditions, such as in SF_6-insulated coaxial transmission line, which is generally a nearly ideal high frequency cable with very low losses, the signal may be preserved almost intact, so that a signal which has a pulse width of about 1 ns at the point of origin will have suffered little attenuation or dispersion at the point of detection. High voltage solid dielectric or fluid impregnated laminar dielectric cable causes substantial alteration of the PD pulse as a result of high frequency attenuation which is caused by dielectric loss in the insulation, and losses in the conductor and ground semiconducting layers [1]. For

such a cable, the shape of the pulse depends strongly on the distance between the signal-generating void and the end of the cable at which PD detection is taking place.

Frequency-Dependent Cable Attenuation

For XLPE shielded distribution cable, which has been the main subject of field PD measurements, high frequency attenuation is caused mainly by the shield layers [2] and, in the case of transmission class cables, semiconductive bedding layers. While the properties of cable shields can vary widely, they typically have conductivity in the range of 0.1 to 1 S/m and a relative dielectric constant in the MHz range of a few hundred. Figure 6 shows measured attenuation data for two, 15 kV class concentric neutral XLPE distribution cables, one a 22 year old XLPE cable removed from service and the other a recently manufactured TR-XLPE cable. The measured attenuation for the 22 year old XLPE cable is very noisy as a result of its short length; however, the frequency dependent attenuation of the two cables is clearly very similar. From a wide range of past measurements, the attenuation of such cables, which can be written as 4 to 6 $x10^{-11}\omega$ Nepers/m, where ω is radial frequency, a range which will be adopted in the discussion below. Since analytic equations will be provided for all parameters of interest, other attenuations could be substituted, as appropriate.

The propagation velocity of a coaxial XLPE insulated signal cable is 0.67 c ($c/\sqrt{2.25}$). The propagation velocity of an XLPE insulated power cable is in the range of 0.58 c. The difference is caused by the high dielectric constant of the shields, which, at high frequency, act as lossy, high dielectric constant dielectrics which cause attenuation, decrease the propagation velocity, and cause dispersion as a result of their frequency-dependent dielectric constant.

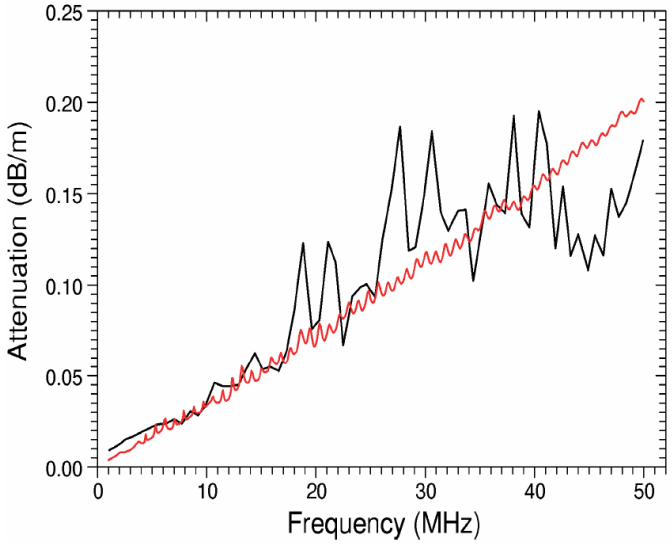

Figure 6. Measured attenuation for two 15 kV class concentric neutral XLPE cables. The black line provides the measured attenuation of a 22 year old XLPE cable while the red line provides the attenuation of a recent TR-XLPE cable. The measurement of the older cable is noisy as the sample was rather short.

Measured Data for High Frequency Attenuation

For solid dielectric cable, which is the main subject of PD measurements in distribution systems, high frequency attenuation is caused mainly by the shield layers [2-4]. While the properties of cable shields can vary widely, they typically have conductivity in the range of 0.1 to 1 S/m and a relative dielectric constant in the MHz range of a few hundred. Most importantly, the attenuation can be modeled as proportional to frequency, and this allows an analytic solution for PD pulse attenuation as a function of distance, as will be shown below.

Table 1 shows the attenuation constant as determined from measurements on distribution cable. For XLPE cable, the measured attenuation constant varies from 3.28×10^{-11} Nepers-s/m to 6.14×10^{-11} Nepers-s/m, where the attenuation at frequency ω is given by $\exp(-\alpha\omega L)$, where α is the attenuation constant in Nepers-s/m, ω is the radial frequency, and L is the distance propagated.

Table 1: Measured Attenuation Constants

Voltage	Dielectric	Ground	Attenuation Constant	Ref
15 kV	PILC, singe phase	Pb	2.17E-10	Boggs
10 kV	PILC, 3 cond	Pb	1.1 to 1.5E-10	[5]
15 kV	EPR1	Cu Tape	4.78E-11	Boggs
15 kV	EPR2	Cu Tape	1.64E-10	Boggs
15 kV	EPR2	10 Neut Wire	9.17E-11	Boggs
15 kV	EPR3	Cu Tape	5.10E-11	Boggs
15 kV	EPR3	6 Neut Wire	8.76E-11	Boggs
15 kV	EPR3	10 Neut Wire	5.50E-11	Boggs
15 kV	EPR3	16 Neut Wire	3.93E-11	Boggs
46 kV	EPR	Cu Tape	7.33E-11	[2]
28 kV	XLPE	Conc Neut	4.35E-11	[2]
15 kV	TR-XLPE	Cu Tape	3.28E-11	Boggs
15 kV	TR-XLPE	10 Neut Wire	6.14E-11	Boggs
24-138	XLPE		4.40E-11	Lemke

In Table 1, the source of the data is identified by reference where the data have been published and by investigator where not. Veen [5] provides many measurements of PILC cable, but since such cable is not our focus, we have provided only the range of his measurements in Table 1. Interestingly, some of the earliest attenuation measurements from 1982 [2] and most recent measurements (Lemke) for XLPE cable are in very good agreement, which suggests that whatever improvements have been made in cable shields has not had a major impact on their dielectric properties.

These measured attenuation data provide a basis for evaluating the range of PD detection sensitivity which is likely to be achieved under field conditions for jacketed cable which is in good condition. The attenuation of unjacketed cable can vary greatly as a result of interm ittent contact between the neutral wires and the ground shield. Based on the data of Table 1, we will use an attenuation constant of 5×10^{-11} s/m as a typical value, although PD detection sensitiv ity will be evaluated as a function of the attenuation constant.

PD Pulse Propagation

Gaussian Pulse

We start by assuming that the PD pulse is generated by a Gaussian current propagating in the conductor, i.e.,

$$I(t) = I_o \exp\left(-\frac{t^2}{2\sigma^2}\right) \tag{1}$$

where I_0 is the peak pulse current amplitude and the pulse width (full width at half maximum or FWHM) is 2.36 σ. The partial discharge magnitude of this pulse is given by

$$Q = \int I(t)\,dt = I_0\,\sigma\sqrt{2\pi} = \frac{V_0\,\sigma\sqrt{2\pi}}{Z} \tag{2}$$

where $V_0 = I_0 Z = I_0 Zc/2$ is the peak voltage and Zc is the cable characteristic impedance. Thus the voltage waveform is

$$V(t) = V_0 \exp\left(-\frac{t^2}{2\sigma^2}\right) = \frac{Q\,Zc}{2\sigma\sqrt{2\pi}} \exp\left(-\frac{t^2}{2\sigma^2}\right) \tag{3}$$

where Q is the partial discharge magnitude (C).

As is well known, the Fourier transform of a Gaussian is a Gaussian,

$$V(\omega) = Q\,Z \exp\left(-\frac{1}{2}\omega^2\,\sigma^2\right) \tag{4}$$

We now multiply the by the frequency dependent attenuation,

$$V_A(\omega) = Q\,Z \exp\left(-\frac{1}{2}\omega^2\,\sigma^2\right) \exp\left(-\omega\alpha L\right) \tag{5}$$

and transform this back into the time domain, obtaining,

$$V_A(t) = \frac{Q\,Zc}{4\sigma\sqrt{2\pi}}\left[\exp\left(A^2\right)\mathrm{erfc}\left(A\right) + \exp\left(B^2\right)\mathrm{erfc}\left(B\right)\right] \tag{6}$$

where erfc is the complimentary error function (1-erf) and

$$A = \left(\frac{\alpha L + jt}{\sqrt{2}\,\sigma}\right),\; B = \left(\frac{\alpha L - jt}{\sqrt{2}\,\sigma}\right) \tag{7}$$

where α is the attenuation factor, L is the distance propagated by the PD pulse, t is time, σ characterizes the initial pulse width as described above, and $j = \sqrt{-1}$.

Equations 6 and 7 give the pulse waveform as a function of distance propagated, attenuation constant, and initial pulse width (2.36 σ full width half maximum [FWHM]). These equations can be difficult to evaluate, as for typical conditions, $\exp(A^2)$ becomes very large at large

distances, while erfc(A) becomes extremely small. However the equation has been evaluated successfully using Maple.

The peak pulse amplitude can be obtained by setting t=0,

$$V_p(L) = \frac{QZc}{2\sigma\sqrt{2\pi}}\left(\exp\left(\frac{\alpha^2 L^2}{2\sigma^2}\right)\mathrm{erfc}\left(\frac{\alpha L}{\sigma\sqrt{2}}\right)\right) \tag{8}$$

As the pulse propagates down the cable, it loses high frequency energy, resulting in a reduction in the optimum bandwidth for detection which can be taken as roughly the -6 dB bandwidth [1]. From eq(5), we can determine the -6 dB bandwidth (Hz) as

$$BW(L) = \frac{-\alpha L + \sqrt{\alpha^2 L^2 + 2\sigma^2 \ln(2)}}{2\pi\sigma^2} \tag{9}$$

so that the -6 dB bandwidth for the 1.2 ns FWHM Gaussian pulse at inception is about 370 MHz, and this decreases to about 20 MHz after propagating roughly 100 m down the cable, which explains why typical detection bandwidths are in the range of 10 to 20 MHz.

As noted above, the Fourier transform of a Gaussian is a Gaussian. In eq(4), this Gaussian in the frequency domain is weighted by the frequency-dependent attenuation in order to compute the attenuated waveform in the time domain. After weighting in the frequency domain, the spectral distribution is no longer Gaussian, which means that in the time domain, the pulse waveform is no longer Gaussian. The waveform after attenuation, eq(6), is a complicated function, and we have not been able to obtain an analytical solution for the pulse width (FWHM) as a function of distance, although a numerical solution is possible, as shown in Figure 2. The pulse width can be approximated by assuming that the pulse after frequency dependent attenuation is Gaussian. In this approximation, the pulse width as a function of distance propagated is given by

$$PW(L) = \frac{2.36\sigma}{\exp\left(\frac{\alpha^2 L^2}{2\sigma^2}\right)\mathrm{erfc}\left(\frac{\alpha L}{\sigma\sqrt{2}}\right)} \tag{10}$$

and the energy in the pulse is given by

$$W(L) = \frac{Q^2 Zc}{4\sigma\sqrt{\pi}}\left[\exp\left(\frac{\alpha^2 L^2}{2\sigma^2}\right)\mathrm{erfc}\left(\frac{\alpha L}{\sigma\sqrt{2}}\right)\right]. \tag{11}$$

Asymmetric PD Pulse

Many PD pulses are asymmetric, with a waveform similar to the measured waveform shown in Figure 7 [6]. In order to carry out the above analysis for such a waveform, we create an analytic waveform from a sum of Gaussians, and since the above analysis can be carried out for each Gaussian component of the waveform, we can sum the result to produce the PD pulse as a function of distance propagated. As high frequencies are attenuated more rapidly than low frequencies, the pulse will become increasingly symmetric as a function of distance propagated.

We therefore model the measured PD waveform of Figure 1 as a sum of Gaussians, a plot of which is also shown in Figure 1,

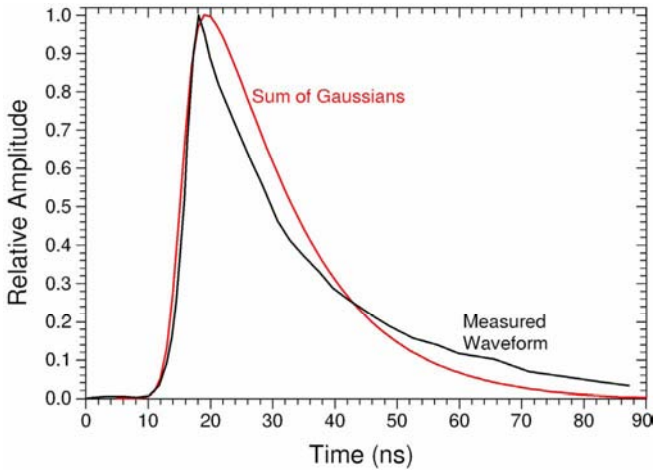

Figure 7. Measured asymmetric PD waveform provided by Prof. Lemke along with the sum of Gaussians used to simulate the measured waveform [6].

$$I(t) = I_0 \sum_{i=1}^{60} \left(A_0(i) \exp\left(-\frac{(t - t_0(i))^2}{2\sigma_0(i)^2} \right) \right) \text{ where} \tag{12}$$

$$A_0(i) = \frac{0.2245}{\sqrt{\exp\left(\frac{i}{5}\right)}},\ \sigma_0(i) = 10^{-9} \frac{\exp\left(i^{0.25}\right)}{\sqrt{2}},\ t_0(i) = \frac{i + 5000}{10^9}$$

which results in a peak current of I_0 and a charge of $2.15 \times 10^{-8}\ I_0$.

The pulse charge (time integral of current) can be written as

$$Q = \int I(t)\,dt = \sum_{i=1}^{60} I_0 A_0(i) \sigma_0(i) \sqrt{2\pi}\,, \text{ or} \tag{13}$$

$$Q = \sum_{i=1}^{60} \frac{V_0 A_0(i) \sigma_0(i) \sqrt{2\pi}}{Z} \tag{14}$$

(14)

where $V_0 = I_0 Z = I_0 Zc/2$. Thus the voltage waveform is

$$V(t) = V_0 \sum_{i=1}^{60} \left(A_0(i) \exp\left(-\frac{(t - t_0(i))^2}{2\sigma_0(i)^2} \right) \right) \tag{15}$$

We can compute the waveform as a function of distance propagated by noting that for each Gaussian in the sum, we can take a Fourier transform, multiply by the cable attenuation, and transform back into the time domain, as was implemented for a single Gaussian PD pulse above (eq(6)). Thus the waveform after propagating a distance L is just the sum of the resulting waveforms after this process. As noted above, eq(6) is difficult to evaluate as it consists of sum of products of very large numbers times very small numbers. We can develop an approximate solution by assuming that the attenuated Gaussian components remain Gaussian with a distance-

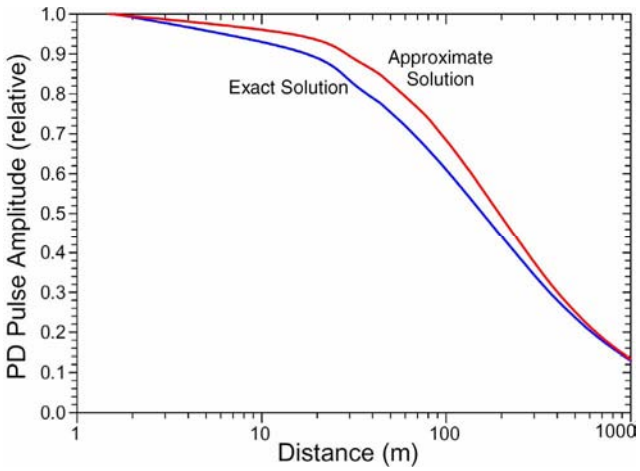

Figure 8. Asymmetric PD pulse amplitude as a function of distance propagated for the exact and approximate solutions with an attenuation constant of $5x10^{-11}$ s/m. The approximate solution appears to be accurate to within 10% over the full range of distance.

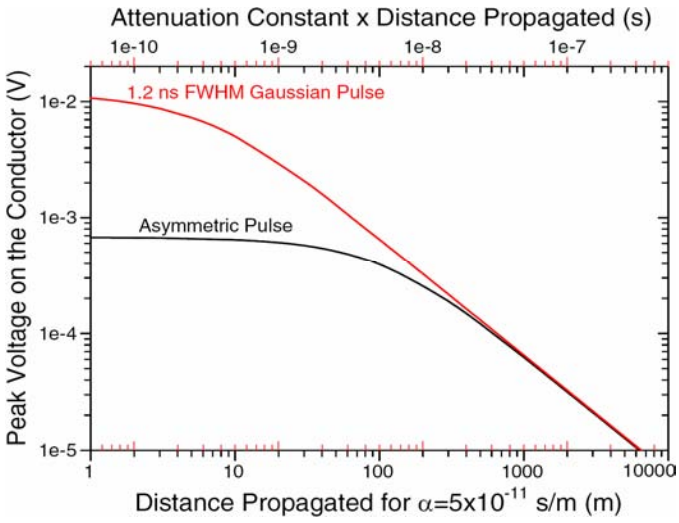

Figure 9. Peak voltage on the conductor for a 1 Gaussian PD pulse and a 1 pC asymmetric PD pulse propagating on a cable with a 30 Ω characteristic impedance. Beyond a few hundred metres, the pulse amplitudes merge, as the total charge in each pulse is the same, and the effective bandwidth is small compared to the initial bandwidth of either pulse.

dependent standard deviation of eq(16) and amplitude of eq(17), which results in an approximate waveform given by eq(18).

$$\sigma_i(L) = \frac{\sigma_0(i)}{\exp\left(\frac{\alpha^2 L^2}{2\sigma(i)^2}\right)\operatorname{erfc}\left(\frac{\alpha L}{\sigma_0(i)\sqrt{2}}\right)} \tag{16}$$

$$A_i(L) = A_0(i)\left(\exp\left(\frac{\alpha^2 L^2}{2\sigma(i)^2}\right)\operatorname{erfc}\left(\frac{\alpha L}{\sigma_0(i)\sqrt{2}}\right)\right) \tag{17}$$

$$V(t,L) = V_0\sum_{i=1}^{60}\left(A_i(i)\exp\left(-\frac{(t-t_0(i))^2}{2\sigma_i(L)^2}\right)\right). \tag{18}$$

Figure 8 shows the pulse amplitude as a function of distance propagated for the asymmetric pulse based on the exact solution and the approximation of eq(18). The approximate solution of eq(18) appears to be accurate to within 10% over the full range of distance, which is adequate for the purposes of PD detection.

This process can be applied to any waveform which can be written as a sum of Gaussians, and essentially waveform can be written as a sum of Gaussians, from triangular waveforms to rectangular pulses. Thus this approach provides a very general formulation for propagation of an essentially arbitrary pulse on a shielded cable subject to the assumptions given above, the most important of which is the form of the frequency dependent attenuation.

The PD pulse amplitude for a 1 pC pulse as a function of distance propagated is shown in Figure 9. As would be expected of a broader waveform with longer risetime, the asymmetric PD pulse

attenuates less rapidly at small distances than the much narrower Gaussian PD pulse. Figure 10 shows the -3 dB bandwidths for the Gaussian and asymmetric pulses. In the case of both the

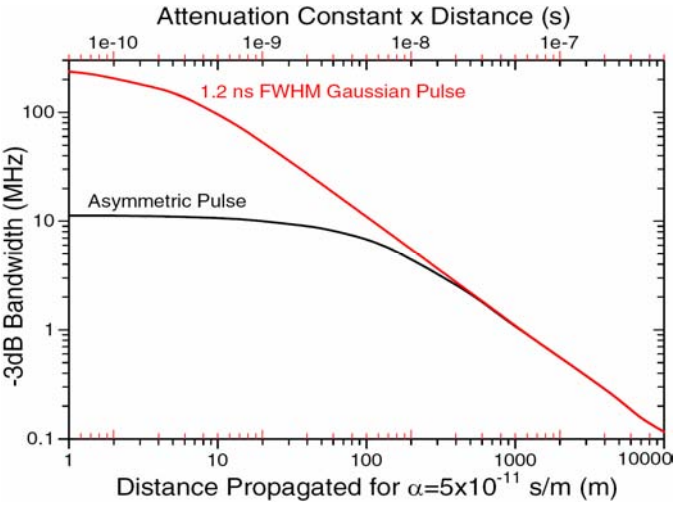

Figure10. -3 dB bandwidth as a function of distance propagated for a 1.2 ns (FWHM) Gaussian PD pulse and an asymmetric PD pulse propagating on a cable with a 30 Ω characteristic impedance and attenuation constant of $5x10^{-11}$ s/m. Beyond a few hundred metres, the bandwidths merge.

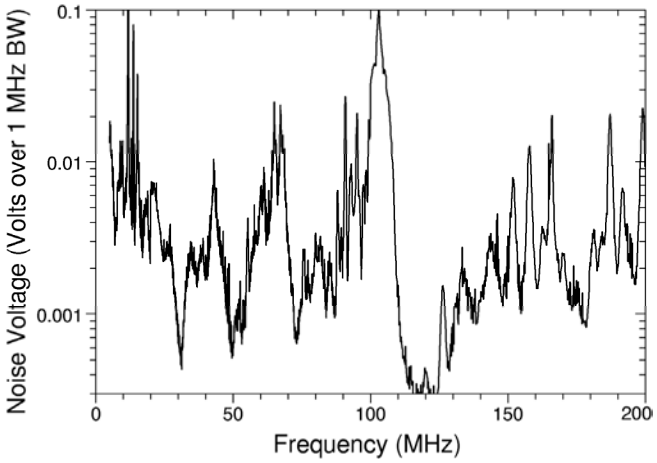

Figure 11. Measured average noise spectrum on cables in urban/industrial environments after correction for PD coupler response and for gain in the measurement electronics. Over the frequency range up to 50 MHz, an average noise floor of about 3 mV seems reasonable. Given a 1 MHz measurement bandwidth, this corresponds to 3 μV/Hz½.

peak amplitude and -3 dB bandwidth, the data for the Gaussian and asymmetric pulses converge for propagation distances greater than a few hundred metres as the pulse shape and bandwidth are dominated by the high frequency attenuation.

Implications for PD Detection

Noise on the Cable

The spectral distribution of noise on the cable during measurement of partial discharge varies depending on the local environment. However we can obtain an idea of the typical noise by averaging over a number of locations and removing the coherent noise sources (radio stations, etc.) and focus on the broad background noise floor. Figure 11 shows such data corrected for the PD coupler response and for the gain in the measurement electronics. These data are measured with a 1 MHz bandwidth. An examination of the data in the range up to 50 MHz suggests a noise floor in the range of 3 mV, which implies a noise voltage density of about 3 μV/√Hz. We will analyze the PD detection sensitivity in terms of an assumed background noise floor of this form.

Gaussian Pulse

As noted in detail in [7], a matched filter is very difficult to implement for detection of partial discharge propagating on a cable, as the waveform changes, which means that a bank of filters is

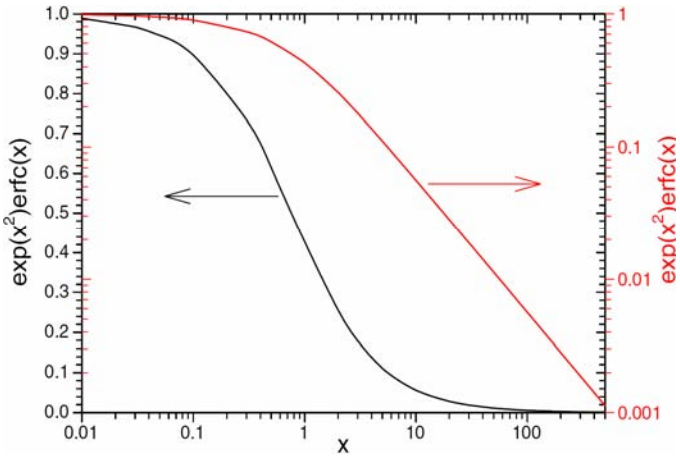

Figure 12. Plot of exp(x^2)erfc(x) over the range relevant to PD detection. The left axis is linear while the right axis plots the same data on a log scale to provide better resolution for small values.

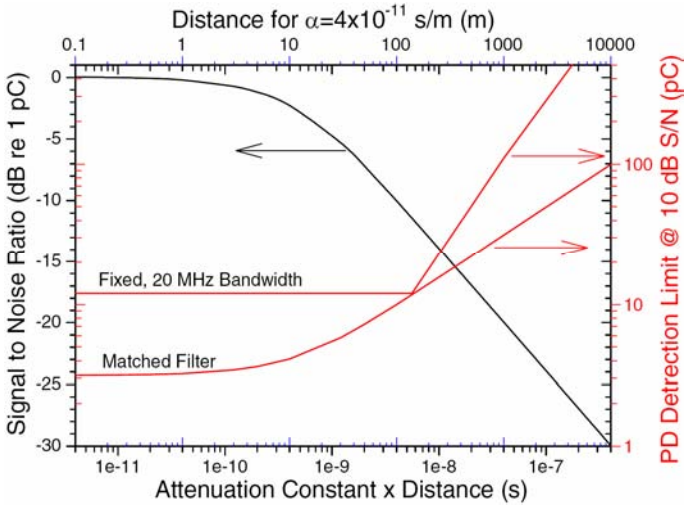

Figure 13. Signal to noise ratio and PD detection sensitivity for 10 dB signal to noise ratio for an assumed noise voltage spectral density of 1 μV/•Hz. The bottom axis is the product of the attenuation constant (s/m) times the distance propagated (m), while the top axis shows distance (m) for an assumed attenuation constant of 4x10^{-11} s/m, which, according to Table 1, is a typical value for XLPE cable. The PD detection sensitivity varies inversely as the square of the noise voltage spectral density, so that a doubling of the noise spectral density to 2 μV/•Hz would reduce the PD detection sensitivity by a factor of 4. Thus the PD detection limit is very sensitive to the background noise. The PD detection limit is shown for the case of a matched filter, for which the bandwidth is a function of the distance propagated, and for a fixed 20 MHz bandwidth, both for a 10 dB S/N.

required, each near optimum for a range of distances propagated. In the case of a Gaussian PD signal propagating in white noise, a rectangular filter of optimum bandwidth comes very close (within about 1 dB) of a matched filter [1]. Thus in this case, the change in the -6 dB bandwidth of the pulse gives an indication of the optimum detection bandwidth.

The signal to noise ratio for a Gaussian pulse detected in white noise is simply W/S, where W is the energy in the pulse, and S is the spectral noise power density (W/Hz). Based on the above discussion, the spectral noise power density for a noise voltage V_n (V/Hz^{½}) is given by $V_n^2/4Zc$, where Zc is the characteristic impedance of the cable. An approximate formula for the energy in the PD pulse as a function of distance propagated has been given in eq(11). The signal to noise ratio for the ideal case, i.e., a matched filter, or equivalently, cross correlation with the known signal waveform, as a function of distance propagated can therefore be approximated by

$$SN(L) = \frac{Q^2 Z^2}{\sigma V_n^2 \sqrt{\pi}} \left[\exp\left(\frac{\alpha^2 L^2}{2\sigma^2} \right) \mathrm{erfc}\left(\frac{\alpha L}{\sigma\sqrt{2}} \right) \right] \qquad (19)$$

The bracketed term in eq(19) is of the form exp(x^2)erfc(x) which is plotted in Figure 6. We can assume that σ is about 5x10^{-10} s which corresponds to a pulse width of about 1.2 ns. Thus given

a value of α, which is likely to range between $3x10^{-11}$ and $1.5x10^{-10}$ s/m for solid dielectric cable, one can plot the signal to noise ratio for any value of V_n ($V/Hz^{½}$). Figure 7 plots the signal to noise ratio for a 1 pC PD pulse ($Q=10^{-12}$ C) for a background noise level of 1 $\mu V/Hz^{½}$, and characteristic impedance of 30 Ω as a function of the product, αL.

We can compute the PD detection sensitivity based on a 10 dB signal to noise ratio as a function of distance propagated by using eq(11) for the energy in the pulse and the above value for S. This results in the "matched filter" detection sensitivity shown in Figure 7. The effective signal bandwidth was presented in Figure 4. The PD detection sensitivity of Figure 7 is based on PD detection using a matched filter (or equivalently cross correlation) or some other technique, such as recording a large quantity of data and extracting the PD signals using wavelet analysis, which does not require triggering on the first voltage PD pulse above the noise. In the case of PD detection based on triggering on the first PD pulse above the noise, the detection sensitivity will be degraded somewhat, as the effective peak noise is about 4 times the RMS noise voltage for the measurement bandwidth. Thus for a 1 pC PD pulse which originates with a pulse width of 1.2 ns, the optimum detection (-6 dB) bandwidth at a detection distance of 100 m is about 20 MHz and the peak voltage amplitude is about 1 mV (Figure 5).

For the assumed noise voltage spectral density of 1 $\mu V/Hz^{½}$ over a bandwidth of 20 MHz, the effective peak noise voltage will be about 18 mV. Thus the PD detection sensitivity will be in the range of 25 pC which compares to about 12 pC in Figure 7. PD detection is normally carried out with a fixed PD detection bandwidth in the range of 20 MHz, as the distance of the PD source from the detector is not known. At small distances from the PD source, the PD detection sensitivity using a fixed PD detection bandwidth suffers because the detection bandwidth is smaller than optimum, so that useful signal is "thrown away", while for large distances from the PD source, sensitivity suffers because the detection bandwidth is greater than optimum, so that noise is being detected without useful signal. As a result, for short distances, the PD detection sensitivity is constant and limited by the detection bandwidth, while for long distances, the PD detection sensitivity degrades more rapidly than the theoretical optimum (matched filter). An estimate of the PD detection sensitivity for a fixed bandwidth of 20 MHz and the conditions discussed in the caption is shown in Figure 7.

Asymmetric Pulse

As can be seen from Figures 9 and 10, beyond about 100 m propagation distance, the Gaussian and asymmetric pulses differ little in amplitude or bandwidth, and the bandwidth of the asymmetric PD pulse is very close to the typical measurement bandwidth of field PD detection/location systems, about 20 MHz. As a result, the PD detection sensitivity for the asymmetric pulse based on a matched filter or similar detection schemSe will be approximately that for the fixed 20 MHz bandwidth in Figure 7 for PD propagation distances up to about 100 m, and beyond 100 m, the PD detection sensitivity should follow the "matched filter" line in Figure 7. For the case of fixed 20 MHz bandwidth, the PD detection sensitivity will be roughly the same as for the narrow Gaussian pulse, as the fixed 20 MHz bandwidth essentially turns the narrow pulse into one with a width and amplitude similar to the asymmetric pulse.

Summary

The above analysis provides a basis for estimating the PD detection sensitivity as a function of distance, background noise, and cable attenuation constant, which, based on Table 1, can vary from about $3x10^{-11}$ s/m to $2x10^{-10}$ s/m. This roughly order of magnitude variation in attenuation constant translates into an order of magnitude variation in the distance over which a PD pulse can be detected, as the attenuation constant enters all the equations as a product with distance. The measured data for XLPE cable (both TR-XLPE and XLPE) vary from $3.3x10^{-11}$ to $6.15x10^{-11}$ s/m, although the attenuation could increase if the number of neutral wires were reduced. Thus XLPE cable can probably vary from about $3x10^{-11}$ s/m to $9x10^{-11}$ s/m. EPR cables are likely to have somewhat greater attenuation, and the measured data range from $3.9x10^{-11}$ to $1.6x10^{-10}$ s/m. The attenuation of PILC cable is even greater. Cables with Cu tape shields tend to have greater attenuation than those with concentric neutrals, and the measured data are for new cables. With field aging of the Cu tape, the conduction across the laps is likely to decrease, resulting in increased attenuation and decreased propagation velocity. The spiraling of the return current down the Cu tape will also cause an axial magnetic field which will induce eddy current in the conductor, resulting in additional attenuation.

All of the data presented are for jacketed cables, where the metallic ground shield is held against the ground shield semicon by the jacket. The attenuation of unjacketed cables is difficult to assess or predict, as the concentric neutral wires will make only intermittent contact with the ground shield, and the attenuation will depend on both the frequency of such contact and the average distance (capacitance) of the neutral wires to the ground shield.

PD Location

In many cases, PD location is nearly as important as detection. The subject of PD location has been examined exhaustively by Steiner, Reynolds and Weeks [5] A reasonably good S/N ratio is required for accurate PD location. For a Gaussian pulse in white noise, the standard deviation of the measured pulse arrival time is given by [6]

$$\Delta = \frac{\sigma\sqrt{2}}{\sqrt{\eta}} \tag{20}$$

where, as usual, σ is the Gaussian pulse standard deviation which characterizes the pulse width, and η is the signal to noise ratio. After propagating 1000 m, the pulse width is in the range of 220 ns (σ=~90 ns) according to eq(10) or nearly 200 times greater than the initial PD pulse. According to eq(20), the standard deviation in the time of arrival will be about 70 ns for a S/N ratio of 10 dB (3.16), which corresponds to a propagation distance of about 10 m (35 ft). To achieve reasonable location accuracy, a S/N in the range of 40 dB (100) is required which would result in a standard deviation of 13 ns. Of course the standard deviation can be reduced by averaging multiple independent measurements. Thus as the pulse spreads, the PD detection S/N must increase in order to maintain reasonable PD location accuracy. This decreases the effective PD detection sensitivity insofar as PD location is required.

Conclusions

A general analytic approach has been developed for predicting the propagation characteristics of PD pulses of arbitrary shape, as well as the partial discharge detection sensitivity which can be achieved for such PD pulse waveforms. The approach has been applied to two typical waveforms, a narrow Gaussian pulse, and a slower, asymmetric pulse. Graphs are presented in a generic form in terms of the product of distance propagated and attenuation constant for an easily scaled background noise, so that the PD propagation characteristics and detection sensitivity can be determined for any parameters of interest.

For both narrow Gaussian and broader asymmetric PD pulses, the PD detection sensitivity under relatively noisy field conditions is likely to be in the range of 30 to 100 pC at 1000 m based on a background voltage spectral noise density of 1 $\mu V/\sqrt{Hz}$. Since the PD detection sensitivity scales as the square of the voltage spectral noise density, the PD detection sensitivity achieved in the field is very sensitive to ambient noise conditions.

References

1. S.A. Boggs and G.C Stone. "Fundamental Limits to the Measurement of Corona and Partial Discharge". IEEE Trans EI-17, No. 2, April 1982. pp. 143-150.
2. G.C. Stone and S.A. Boggs. "Propagation of Partial Discharge Pulses in Shielded Power Cable." 1982 Annual Report of the Conference on Electric Insulation and Dielectric Phenomena, National Academy of Science, Washington, DC. pp. 275-280..
3. Chunchuan Xu, S.A.Boggs, Liming Zhou, and Yingneng Zhou. "High Frequency Properties of Shielded Power Cable, Part 1: Overview of Mechanisms." IEEE Electrical Insulation Magazine. V21 Issue 6, pp.24-28 2005
4. Chunchuan Xu and S.A.Boggs, "High Frequency Loss from Neutral Wire-Shield Interaction of Shielded Power Cable" Submitted to IEEE Trans PD.
5. J. Veen, On-line Signal Analysis of Partial Discharges in Medium Voltage Power Cables. Ph.D. thesis, Technische Universiteit Eindhoven, 2005.
6. E. Lemke and T. Strehl, W. Weissenberg, and J. Herron. "Practical Experiences in on-site PD Diagnosis Tests of HV Power Cable Accessories in Service". Conference record of the 2006 IEEE International Symposium on Electrical Insulation. pp. 498-501.
7. J. Veen, and PCJM van der Wiellen. "The Application of Matched filters to PD Detection and Localization". IEEE Electrical Insulation Magazine, Vol. 19, No. 5, Sep-Oct 2003. pp. 20-26.
8. Eberhard Lemke. Private communication, 2006.

3

REVIEW OF PUBLISHED LITERATURE

Introduction

Most of the published literature related to PD detection and monitoring of transmission class solid dielectric cable relates to solid dielectric cable and especially splices therein. This is not surprising, as the first generation of splices were fabricated in the field, required meticulous workmanship, and were not very reliable. For the most part, these systems concentrated on detection of PD in the joints as this was by far the largest cause of cable failure. Although silicone rubber based cold shrink joints are now becoming available up UHV voltages, the literature continues to focus on PD detection in joints. In addition, most of the published PD detection technology is based on installation of PD couplers within the splices, although other approaches have been taken, such as placing CT's on ground leads. However these approaches tend to be much less sensitive than capacitance couplers installed in the splices or on cable immediately adjacent to the splices.

PD Detection at Splices Using Capacitive Sensors

VHF PD Detection at Splice

Two excellent papers have been published on PD detection based on capacitive couplers installed at or adjacent to splices [1,2]. However, the approaches differ substantially in their details, bandwidth, and intent. The work of Pommerenke [1] has focused exclusively on PD detection in splices employing very wideband PD detection, as the PD coupler is very close to the source of the PD. During his Ph,D. studies, Pommerenke undertook electrodynamic modeling of splices to quantify PD detection sensitivity as a function of PD source location within the splice [3]. His preferred approach is to use differential couplers installed on or adjacent to the splice. These couplers, as those described in [2] involve applying a metal electrode over the cable or splice semicon, which is then insulated and covered by the metalic cable shield. This forms a capacitive coupler, although one with the complex, frequency dependent impedance of the semicon to ground (the cable shield) which results in a high pass characteristic for the coupler. However the high pass characteristic is not highly predictable and will change with temperature and time as a result of changes in the semicon impedance characteristics. On the other hand, the high pass characteristics can be controlled to some degree by the topology of the coupler. The semicon impedance also appears between the metal electrode and the cable conductor; however, the semicon impedance is much less than that of the dielectric and therefore has little effect on the frequency response of the coupler.

Pommerenke employs couplers at either side of the splice to implement a detection scheme which can differentiate between PD coming from within the splice and that coming from the cable. In addition to high frequency attenuation in the cable, the high frequency characteristics

of the coupler also tend to reduce sensitivity to PD pulses coming from outside the splice. Pommerenke's PD detection scheme achieves a sensitivity in the range of 1 pC for PD in or very near the splice. Detection sensitivity drops off rapidly away from the splice as a result of the high pass characteristics of the coupler which contribute to the very high sensitivity for PD in or near the splice.

RF PD Detection Centered on Splice

Fruth [2] takes a similar approach using similar (but not directional) capacitive couplers, but with a different emphasis. Instead of employing a PD detection in the VHF frequency range, he works in the more conventional 1-20 MHz RF range employed for the testing of distribution cable. Fruth assumes that he has simultaneous access to signals from couplers located along the cable so that if a PD signal is common to two cable phases, for example, he can use the common signal from a "clean" phase or location to "gate" out the interfering signal at a location where it interferes with a PD source. In this way but at the cost of greater complexity and the need for an expert operator, Fruth also achieves a PD detection sensitivity in the range of 1 pC under field conditions. However this approach should be applicable to the cable between splices as well as the splices, although sensitivity inevitably "peaks" near the couplers.

Capacitive PD Sensors with Passive Optical Transmission

Lewin [4] took an approach very similar to that of Fruth but employed a Faraday effect optical modulator to encode the PD signal on the light passing through an optical fiber. The system was multiplexed so that only one laser source and GHz bandwidth detector was required, although one electro-optic modulator was required at each PD coupler. The obvious advantage of this approach is that it does not require a power source at each sensor location. This advantage comes as the expense of requiring polarization preserving fiber, electro-optic modulators, etc. The sensitivity achieved by this approach appears to be in the range of 10 pC, about an order of magnitude worse than direct electrical detection. Whether this is a fundamental limitation is not known.

Capacitive PD Sensors at an Insulating Joint

Several investigators have employed PD sensors based on differential detection across an insulating joint [5,6]. In a sense, this approach takes advantage of the break in the conducting shield at an insulating joint to allow high frequency signals to transfer from the conductor-ground shield transmission line to the ground shield-earth transmission line, i.e., from a current flowing on the inside surface of the ground shield to a current flowing on the outside surface of the ground shield. This allows the signal to be picked up by a capacitive sensor to the surface of the shield. Differential or directional detection can be undertaken with a capacitive sensor on each side of the break in the shield. Ota et al. [5] have combined such PD couplers installed at insulating joints (which alternated with non-insulating joints) with local noise gating, gating based on the correlation of the signals at adjacent insulating joints, and use of a spectrum analyzer to select a propitious detection center frequency and bandwidth to achieve a PD detection sensitivity in the range of 10 pC over the full length of a 27 km cable with a sensitivity in the range of 1 pC near the insulating joints on which the capacitive couplers were installed. The system detected one defect during the commissioning tests. Earlier, Katsuta et al. [6] used a

very similar PD couplers at insulating joints and frequency domain detection to achieve a sensitivity in the range of 10 pC over the length of a cable.

Use of CT's Outside the Cable

Numerous authors have employed CT's outside the cable to detect PD. CT's have been applied to the braid over the stress cone of a termination [7], to the connection between the cable shield and the base plate of the termination [7], to ground or cross bonding connections [8], etc. The primary advantage of such approaches is that they can be retrofit to an existing installation. However the sensitivity achieved is generally in the hundreds of pC, well below that obtainable with capacitive sensors in the splices. This might be improved using a variety of noise cancellation techniques, both hardware and software. With wavelet denoising, Lewin et al. [9] achieved a PD detection sensitivity in the range of 10 pC. However wavelet denoising cannot be applied in real time which means that it cannot be used to detect a pulse below the noise unless one is willing to take a "random" snapshot and denoise it. As well, thresholding in wavelet analysis of PD signals has not been automated, although some steps have been taken in that direction.

Heizmann et al. [10] employed a simple single turn CT on the braid between the cable shield and splice body of an insulating joint to achieve PD coupling in the 12 to 40 MHz range. PD was detected in both the frequency and time domain using the spectrum analyzier as a frequency selective filter. A sensitivity of about 4 pC was achieved in the laboratory and about 15 pC under field conditions for PD sources close to the sensor (i.e., in the splice).

Summary

The above review mentions only those papers which had something useful to say about the subject, which constitutes a minority of the roughly 30 papers which were reviewed. Capacitive coupling appears to have provided greater sensitivity than inductive coupling, with state-of-the-art sensitivity of about 1 pC achieved for PD close to the point of detection and a sensitivity of about 10 pC achieved for PD anywhere along a cable which included PD sensors at alternative (i.e., insulating) joints. This agrees reasonably with the theory presented above in section 2.

References

1 Pommerenke, D., T. Strehl, R. Heinrich, W. Kalkner, F. Schmidt, and W. Weissenberg. "Discrimination between Internal PD and Other Pulses Using Directional Coupling Sensors on HV Cable Systems". IEEE Trans DEI, Vol. 6, No. 6, December 1999. pp. 814-824.

2 Henningsen, C.G., K. Polster, B.A. Fruth, and D.W. Gross. "Experience with an On-Line Monitoring System for 400 kV XLPE Cables". Proceedings of the 1996 IEEE Transmission and Distribution Conference. pp. 515-520.

3 Pommerenke, D., R. Jobava, and R. Heinrich. "Numerical Simulation of Partial Discharge Propagation in Cable Joints Using the Finite Difference Time Domain Method". IEEE Electrical Insulation Magazine, Vol. 18, No. 6, November/December 2002. pp. 6-11.

4 Tian, Y., P.L. Lewin, J.S. Wilkinson, S.J. Sutton, and S.G. Swingler. "Continuous On-line Monitoring of Partial Discharges in High Voltage Cables". Conference Record of the 2004 IEEE International Symposium on Electrical Insulation, 19-22 September 2004. pp. 454-457.

5 Ota, H. M. Ichihara, N. Miyamoto, S. Kitai, Y. Maruyama, F. Fukasawa, and H. Takehana. "Application of Advanced After-Laying Test to Long Distance 275 kV XLPE Cable Lines". IEEE Trans PD-10, No. 2, April 1995. pp. 567-579.

6 Katsuta, G., A. Toya, K. Muraoka, T. Endoh, Y. Sekii, and C. Ikeda. "Development of a Method of Partial Discharge Detection in Extra-High Voltage Cross-Linked Polyethylene Insulated Cable Lines". IEEE Trans PD-7, No. 3, July 1992. pp. 1068-1079.

7 Ahmed, N. O. Morel, and N. Srinivas. "Partial Discharge Measurement in Transmission Class Cable Termination". Proceedings of the 1999 IEEE Transmission and Distribution Conference, Volume 1, pp 2-7.

8 Phung, B.T., Z. Liu, T.R. Blackburn, and R.E. Jones. "On-Line Partial Discharge Measurement on High Voltage Power Cables". High Voltage Sympoisum, 22-27 August 1999. IEE Conference Publication No. 467, pp. 4.328.P2-2.332.P2.

9 Tian, Y., P.L. Lewin, A.E. Davies, S.G. Swingler, S.J. Sutton, and G.M Hathaway. "Comparison of On-Line Partial Discharge Detection Methods for HV Cable Joints". IEEE Trans DEI, Vol. 9, No. 4, August 2002. pp. 604-615.

10 Heizmann, Th., Th. Aschwanden, H. Hann, M. Laurent, and L. Ritter. "On-Site Partial Discharge Measurements on Premoulded Cross-Bonding Joints of 170 kV XLPE and EPR Cables". IEEE Trans PD-13, No. 2, April 1998. pp. 330-335.

4

HPFF AND HPGF CABLE

Introduction

Large PD attenuation in HPFF cable is common knowledge although actual measurements of high frequency attenuation appear to be lacking. The reasons for large high frequency attenuation have been attributed to the effect of the pipe, high loss in the cable dielectric, etc. A thorough analysis of the "loss budget" of HPFF cable appears to be lacking. As the understanding of PD pulse propagation in solid dielectric cable has been well developed over the past 25 years,the authors decided to pursue the issue in HPFF cable early in this project.

The authors had an opportunity to spend a couple of days on the floor of the Okonite HPFF and HPGF cable factory in Paterson, NJ during which they were able to observe all stages of HPFF cable manufacture as well as obtain samples of the cable prior to and after impregnation. This provided detailed knowledge of the cable structure, which is summarized below, as well as access to the cables materials in their finished (impregnated) state.

HPFF Cable Structure

Samples of unimpregnated and impregnated 345 kV PPLP cable were obtained. The structure of the cable is as follows:

1. 44 mm diameter (1500 mm^2 or 3000 kcmil) segmental conductor with SS binder tape
2. Conductor shield consisting of four layers of carbon impregnated semiconducting paper tape.
3. 16 mm (600 mils) of PPLP dielectric
4. Two layers of carbon impregnated semicon paper one of which is metalized. The two two layers consist of a semicon tape and the metalized semicon tape with the metal facing outward applied clockwise with a pitch of 34.5 mm and with the semicon layer overlapping the metalized layer by 14.5 mm so that 17 mm of the metalized tape is visible as a stripe down the surface of the unimpregnated cable core with a pitch of 34.5 mm. The metalization has a surface resistivity of 3.7 mΩ/sq which corresponds to 7.14 μm of Al with an assumed conductivity of 3.766×10^7 S/m.

This completes the core of the cable as it is impregnated. After the cable is impregnated, the following layers are added.

5. A layer of metalized PET with the metal facing inward which has a width of 31.5 mm and is applied clockwise with a pitch of 31 (or 31.5) mm.
6. A second layer of metalized PET with the metal facing outward which is co-applied with the same pitch and with the outward facing layer overlapping the inward facing layer by 18 mm.

7. A stainless steel layer of width 31.5 mm applied counter clockwise with a pitch of 36 mm. The SS tape has an effective surface resistivity of 5.68 mΩ/sq given its thickness of 160 μm (6.3 mils). The tape conductivity is $1.1x10^6$ S/m.
8. A 31.5 mm wide metalized PET tape with the metal facing inward which is co-applied with the SS layer with the SS, This PET layer has a surface resistivity of 3.15 mΩ/sq or a conductor thickness of 8.4 μm of Al. The PET layer overlaps the SS layer by 14 mm. Thus the combined tape has an effective width of 49 mm and is applied counter clockwise at a pitch of 36 mm. Note that these two tapes are applied in the opposite direction from all previous tapes in the ground shield structure.
9. Two skid wires, evenly separated, each applied at a pitch of 89 mm (3.5 inches).

PPLP High Frequency Properties

The dielectric properties of the PPLP were measured from 100 Hz to 100 MHz using two Agilent impedance analyzers. The high frequency impedance analyzer is optimized for an impedance of 50 Ω. As the PPLP looks mostly like a capacitor, two samples of differing area were used, with the larger area used from 1 MHz to 20 MHz and the smaller area used from 10 MHz to 100 MHz in order to achieve reasonable accuracy over the entire range. A single layer of impregnated PPLP dielectric was taken from the cable and mounted between two strips of Cu clad glass epoxy circuit board of the same width as the PPLP (31.5 mm) with the polished Cu surface facing the PPLP dielectric. A piece of Cu foil was soldered to the bottom edge of each piece of circuit board, folded over the back of the circuit board and used as the contact for a high frequency measurement fixture. In the case of measurements from 100 Hz to 10 kHz, a standard capacitance fixture was employed.

Figures 14 and 15 show tan(δ) and the relative dielectric constant of the PPLP from 100 Hz to 100 MHz. No data were collected from 100 kHz to 1 MHz, so the straight line in each graph is simply an interpolation. The three samples were used for these measurements, one from 100 Hz to 100 kHz, one from 1 MHz to 10 MHz, and one from 10 MHz to 100 MHz. The decrease in dielectric loss above about 30 MHz is probably an artifact caused by increasing skin effect resistance and the size of the sample. On the basis of these measurements, the average high frequency loss of the PPLP dielectric in the range above 1 MHz appears to be about 0.0095. Over a number of high frequency measurements, the dielectric constant above 1 MHz was lower than measured between 100 Hz and 100 kHz. Again, no data were measured between 100 kHz and 1 MHz, so the line between those points is an interpolation. The step in the dielectric constant at 10 MHz is caused by the change in sample, although one would prefer not to see such a step. The increase in dielectric constant above about 30 MHz ties in with the decrease in dielectric constant, both caused by the large sample size and increasing skin effect resistance.

Carbon Impregnated Paper Semicon Properties

The dielectric properties of the carbon impregnated paper semicon were measured using semicon tapes removed from the oil-impregnated cable sample. Interestingly, the thickness of the oil-impregnated semicon paper was 140 μm (5.5 mils) while the thickness of the unimpregnated semicons was 178 μm (7 mils). The unimpregnated semicon has not been dried and might be swollen with moisture. The dielectric properties of the oil-impregnated semicon paper are shown

in Figures 16 and 17. The dielectric constant is very low compared to a solid dielectric semicon, as is the conductivity.

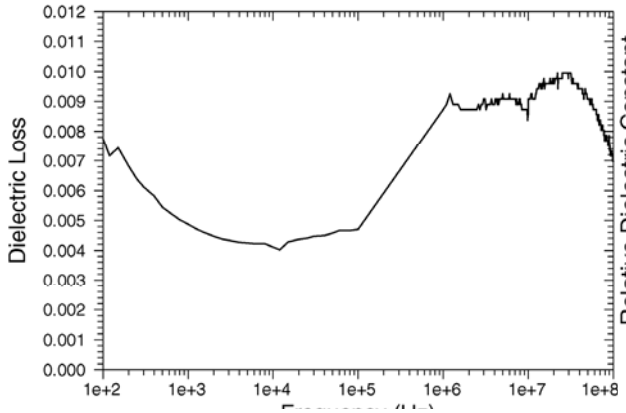

Figure 14. PPLP dielectric loss (tan(δ)) as a function of frequency from 100 Hz to 100 MHz. No data were collected from 100 kHz to 1 MHz, so the straight line is simply an interpolation. The three samples were used, one from 100 Hz to 100 kHz, one from 1 MHz to 10 MHz, and one from 10 MHz to 100 MHz. The decrease in dielectric loss above about 30 MHz is probably an artifact caused by increasing skin effect resistance and the size of the sample. On the basis of these measurements, the average high frequency loss of the PPLP dielectric in the range above 1 MHz appears to be about 0.0095.

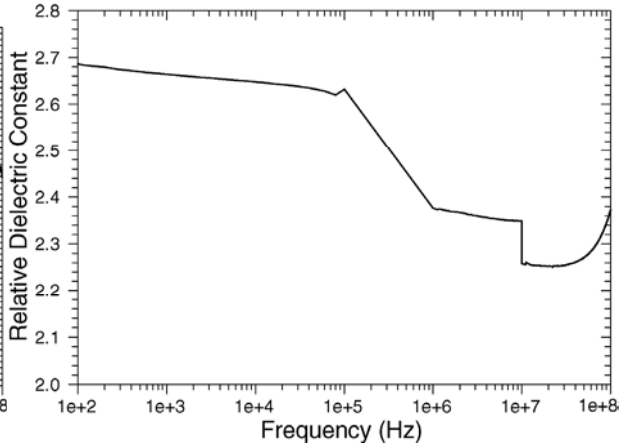

Figure 15. PPLP relative dielectric constant from 100 Hz to 100 MHz. Over a number of high frequency measurements, the dielectric constant above 1 MHz was lower than measured between 100 Hz and 100 kHz. Again, no data were measured between 100 kHz and 1 MHz, so the line between those points is an interpolation. The step at 10 MHz is caused by the change in sample, although one would prefer not to see such a step. The increase in dielectric constant above about 30 MHz ties in with the decrease in dielectric constant, both caused by the large sample size and increasing skin effect resistance.

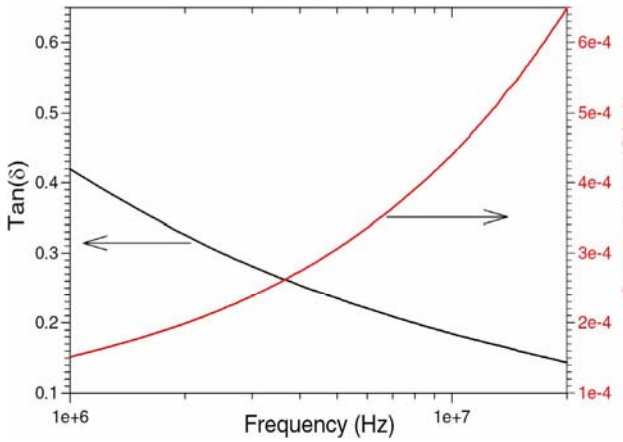

Figure 16. Tan(δ) and conductivity computed therefrom for an carbon impregnated paper semicon taken from an oil-impregnated 345 kV PPLP cable.

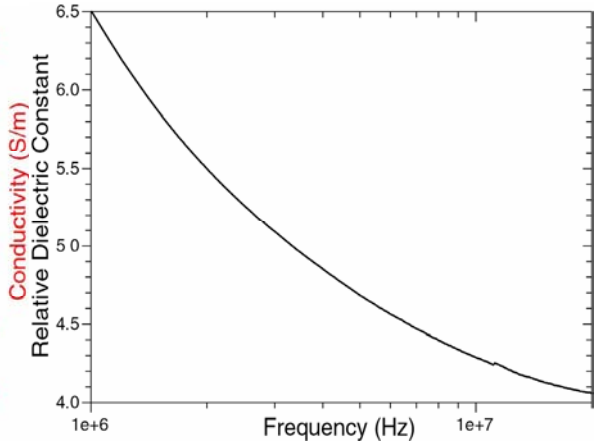

Figure 17. Relative dielectric constant for an carbon impregnated paper semicon taken from an oil-impregnated 345 kV PPLP cable.

Theory of a Lossy Coaxial Cable

The power loss in coaxial transmission line can be expressed as

$$P(z) = P_0(z)\exp(-2\gamma z) \text{ where} \tag{21}$$

$$\gamma = \frac{1}{2}\left[R\left(\frac{C}{L}\right)^{\frac{1}{2}} + G\left(\frac{L}{C}\right)^{\frac{1}{2}} \right] \tag{22}$$

where L, C, R, and G are the cable inductance, capacitance, series resistance, and shunt conductance (admittance) per unit length. This can be rearranged to

$$\gamma = \frac{1}{2}\left[\frac{R}{Z_C} + 2\pi f C Z_C \tan(\delta) \right] \tag{23}$$

where Z_C is the cable characteristic impedance (about 21.5 Ohms at high frequency), R is the AC series resistance of the conductors, f is frequency and tan(δ) is the loss of the dielectric. The attenuation constant, γ, has two terms, one caused by the AC series resistance of the conductors and the other caused by the dielectric loss of the semiconducting layers and the insulation. We can therefore evaluate these loss components separately.

Contribution of the Semiconducting Layers

The shield layers dominate high frequency loss in solid dielectric cable as a result of the high frequency radial displacement (capacitive) current passing through shields and the low loss of the dielectric. At a given frequency, the shield loss is maximized by making the resistive impedance equal to the capacitive impedance of the shield layer. Thus as the dielectric constant of the shield is decreased, the optimum resistance at any frequency will increase, which increases the shield loss.

The capacitive impedance of the dielectric is much greater than the impedance of the shield layers. Thus the dielectric layer can be considered a current limiting impedance in series with the shield layers. To a very good approximation, the loss in the shield layers can be computed by calculating the capacitive current through the dielectric while ignoring the shield layers and then computing the loss in the shield layers caused by this current, recognizing that the shield layer impedances are complex. Using this approach, we find the frequency dependent attenuation shown in Figure 18. The shield-induced attenuation is very modest and typical of solid dielectric cable.

Conductor AC Resistance

The skin depth of a conductor is given by

$$\delta = \sqrt{\frac{2}{2\pi f \mu \sigma}} \tag{24}$$

where μ is permeability (H/m), *f* is frequency (Hz), and σ is conductivity (S/m). For a round conductor which is much thicker than its skin depth, the AC resistance is just the DC resistance of the surface layer one skin depth deep. Thus in the case of the conductor, the AC resistance at 10 MHz is about 5.9 mΩ/m and scales as the square root of frequency.

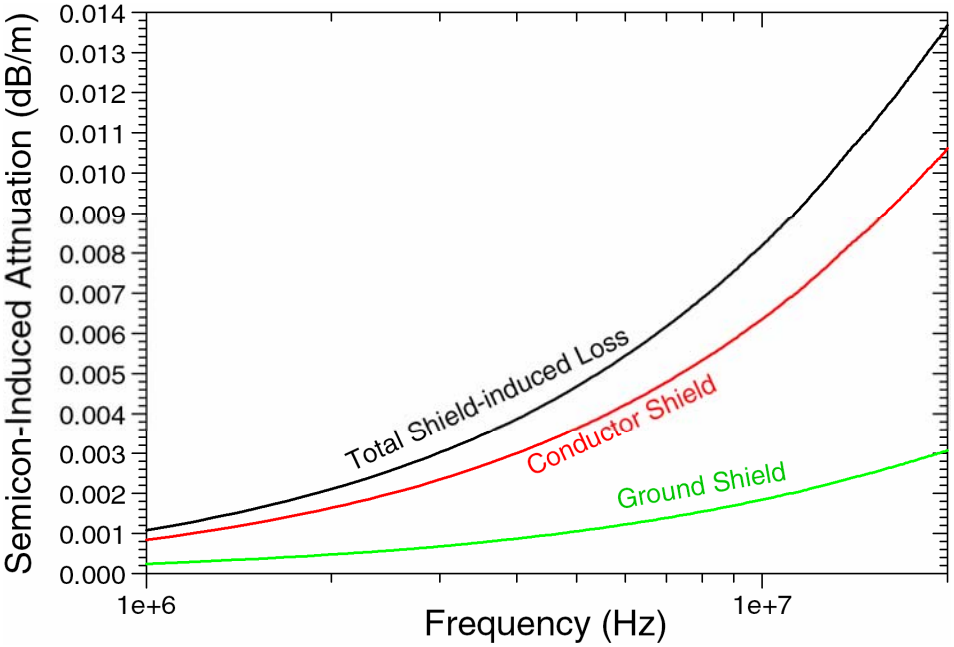

Figure 18. High frequency attenuation caused by conductor and ground shields based on the measured shield impedance data shown in Figures 18 and 19. The computed loss is typical of shield loss in solid dielectric cable.

The shield is more complex. The skin depth of Al at 10 MHz is about 26 μm while that of stainless steel is about 150 μm. Thus the SS tape, at 160 μm is comparable to its skin depth at 10 MHz, and the two Al clad tapes facing each other (17 μm) is comparable to the skin depth of Al at 10 MHz. A rather complex formula which involves complex Bessel functions must be used to compute correctly the AC resistance of a metal layer which has a thickness comparable to the skin depth. Another issue related to the shield is whether the current flows straight down the shield or spirals down the 5 conducting layers, three of which are applied in one direction (CW) and two of which were applied in the opposite direction (CCW).

Also, the skid wires connect to these conducting layers and also to the pipe at locations where the epoxy coating on the inside of the pipe has been damaged during handling or pulling of the cable. The pipe AC conductivity is a strong function of its permeability. One reasonable assumption would be that the magnetic coercivity of the pipe is overcome by the AC current, as in the bias field of an audio tape recorder, so that the high frequency permeability of the pipe is that seen by the AC current, which would be in the range of 1000 μ_0. For such a permeability, the resistance of the pipe is about 37 mΩ/m at 10 MHz, which is large compared to that of the conductor.

Given the many uncertainties, we adopt two extreme assumptions with respect to the ground shield resistance, viz., (i) that the current flows straight down the ground shield and the layers are

fully penetrated and (ii) that the current spirals down the layers, which are again fully penetrated. The first assumption results in a ground shield resistance of 3 mΩ/m. If we were to assume that the three Al layers formed a single layer which was penetrated only to 1 skin depth, then the ground shield resistance would be about 7 mΩ/m without any current flowing in the SS tape.

If we assume that the current spirals down the shield conductors, as probably does occur to some degree, any axial magnetic field would cause a large eddy current loss at the conductor which would imply a large AC resistance. As a result, the current would probably distribute between the CCW and CW layers so as to cancel the axial magnetic field at the conductor. Based on this assumption, the shield resistance would be about 22 mΩ/m as a result of the increased length of the ground path, which is still less than the pipe AC resistance. Given the complex lay of the various conductors, the current probably has a complex path which is much shorter than following the spiral lay. As a result, the return current from a PD pulse probably follows the shield layers rather than transfers to the pipe.

HPFF High Frequency Loss

Based on the above, we can produce Figure 21, which shows the various loss components. The large uncertainty is shield loss. The PPLP dielectric dominates the loss over most of the frequency range, and this loss component should be reasonably accurate. Based on this loss, alone, PD detection above about 10 MHz is not likely, as the high frequency loss over a distance of 500 m (1500 ft) would be in the range of 30 dB (roughly a factor of 30). However the dielectric loss in the MHz region, around 0.01 dB/m, is not excessive. The large uncertainty in predicting high frequency HPFF cable loss results from the complex ground conductor structure, and the only way to determine the loss with any certainty is to make loss measurements on impregnated HPFF cable, as described below.

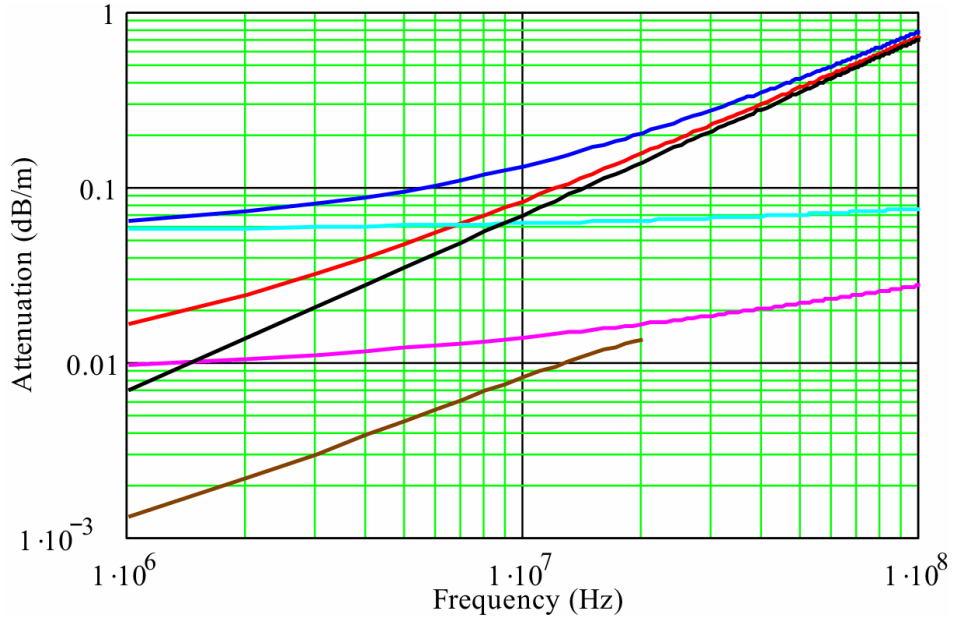

Figure 19. Various loss components of HPFF cable, including:
Black: Loss from the PPLP dielectric
Purple: Loss from the shield assuming full penetration and axial flow.
Light Blue: loss from the shield assuming full penetration but spiral flow.

Red: Total loss based on straight current flow in the fully penetrated shield.
Dark Blue: Total loss based on spiral flow in the fully penetrated shield.
Brown: Total loss from conductor and ground semiconducting shield layers

Measured Attenuation of HPFF Cable

Measurements were carried out on a 450 ft length of single phase PPLP cable on a reel at the Okonite factory in Patterson, NJ. The cable was complete to the skid wires. As a result of the large high frequency attenuation combined with the relatively long length tested, measurement was not possible beyond 40 MHz. Figure 20 shows results of the measurement in comparison with a 15 kV TR-XLPE concentric neutral cable. The loss of the PPLP cable is much greater than that of the concentric neutral cable, and the loss at 1 MHz is already quite large, where the loss of the concentric neutral cable at 1 MHz is very small in comparison. Note that the measured loss is in relative good agreement with the computed loss assuming that the current penetrates the ground structure fully and flows straight down the ground structure (red line in Figure 19). At 1 MHz, the measured and predicted loss is about 0.02 dB/m, at 10 MHz, the measured loss is about 0.06 dB/m while the predicted loss is 0.08 dB/m, and at 40 MHz, the measured loss is about 0.2 dB/m while the predicted loss is 0.3 dB/m. Given the large numbers of assumptions required to compute the loss as given in Figure 19, the agreement is not too bad.

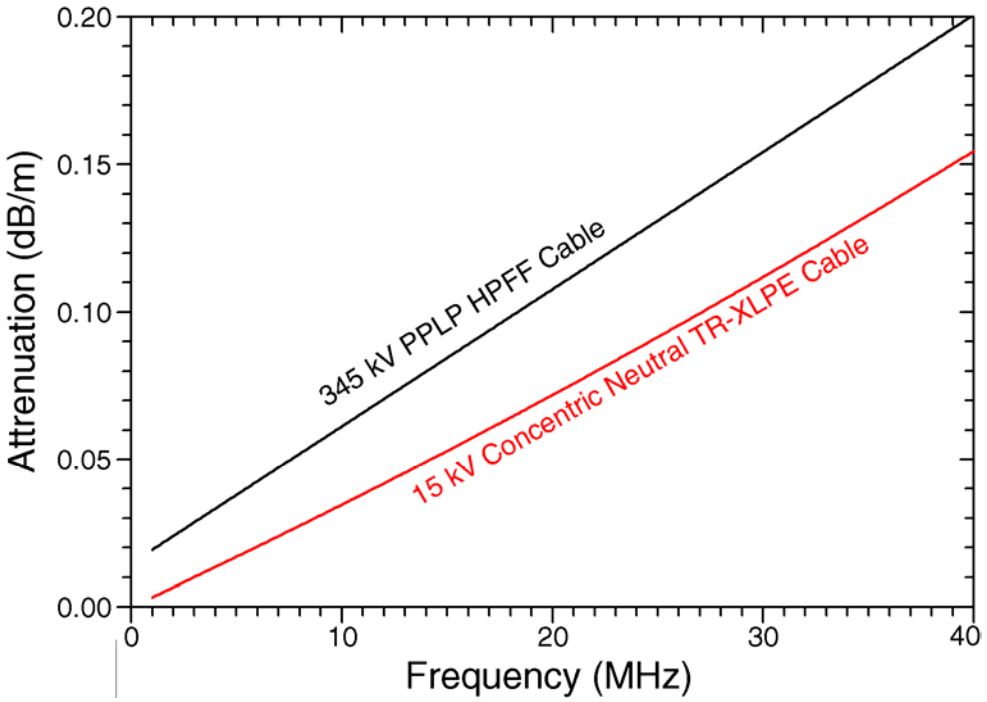

Figure 20. Measured attenuation of 345 kV PPLP cable with 15 kV concentric neutral TR-XLPE cable shown for reference.

The main implication of Figure 20 is that a PD pulse will be attenuated somewhat more than for a typical concentric neutral distribution cable. The large attenuation at 1 MHz, which drops to near zero at power frequency, means that even fairly low frequencies will be attenuated substantially, which implies that the pulse amplitude will continue to drop at large distances much more rapidly than for the XLPE cable. Figure 21 plots the relative peak amplitude as a function of distance propagated for a typical Gaussian PD pulse. Note that for a distribution

class TR-XLPE cable, the PD pulse amplitude tends to level off at large distances as the bandwidth of the pulse decreases in to the region where the cable attenuation is low. However this does not occur for the PPLP cable as a result of the large attenuation in the MHz region.

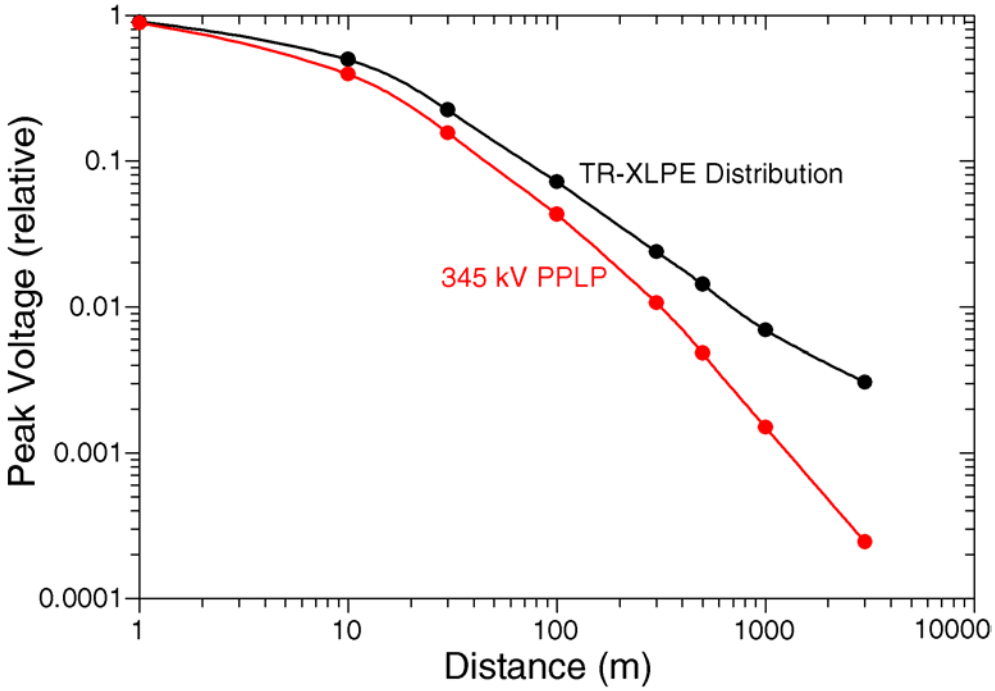

Figure 21. Relative PD pulse amplitude as a function of distance propagated for a Gaussian PD pulse. For a typical solid dielectric distribution cable, the PD pulse amplitude tends to "level off" at large distances as a result of the reduced pulse bandwidth and the reduced cable attenuation at lower frequencies. However, this does not occur for the PPLP cable as a result of its large attenuation in the MHz region.

Conclusions

The above measurements and analysis, which provide reasonably good agreement between computed and measured attenuation for PPLP cable, provide a reasonable basis for understanding the large loss in this cable, which is mainly the result of the high resistance of the ground structure. In a pipe, some of the current in the ground structure might flow through the pipe wall, but this will not reduce the attenuation by much, as the steel pipe has a high permeability which results in a small skin depth. This, combined with the moderate conductivity of the pipe steel, will result in high resistive losses for high frequency currents propagating along the pipe wall. In addition, the inductance is greater for that current path, which favors the current propagating down the cable core ground structure. The result of the high ground structure resistance is the large attenuation see in Figure 21 in comparison with even a relatively high loss TR-XLPE distribution cable.

5

TRANSMISSION CLASS SOLID DIELECTRIC CABLE

Introduction

As discussed in Chapter 2, the high frequency attenuation of distribution cable, including concentric neutral, taped shield, and PILC, is fairly well characterized through measurements and fairly well understood. The same cannot be said for transmission class solid dielectric cable, for which very few if any measurements have been reported. Usually, transmission class solid dielectric cable differs from distribution class cable in being hermetic, i.e., sealed against ingress of moisture. This requires either a corrugated Al or Cu enclosure or a metalized polymermic barrier which is wrapped around the cable core and bonded to itself to provide a moisture barrier. This construction requires semiconductive bedding layers which accommodate the thermal expansion of the XLPE while maintaining electrical continuity between the ground shield semiconductive layer of the cable core and the ground conductor, i.e., concentric neutral wires or corrugated metallic sheath. These bedding layers have no analog in distribution cable and appear to have a substantial impact on the high frequency loss of the cable.

Cable Constructions and Materials

The high frequency propagation characteristics were measured for two cable structures, shown in Figure 22. One cable had a corrugated Cu sheath and was 404 m long, while the other had neutral wires and a laminated metal-polymer tape moisture barrier which was wrapped longitudinally around the cable core, lapped and glued. The latter cable was 565 m long.

The conductor and ground shield materials had measured conductivities of 20 S/m (super smooth) and 10 S/m (firmly bonded), respectively, which were constant from 1 to 100 MHz. This is very high conductivity relatively to a distribution cable shield, where 0.1 to 1 S/m is more typical. The conductivity was sufficiently high that the dielectric constant could not be measured, and the materials were essentially purely resistive over the full range of frequency.

In the case of the corrugated Cu sheath cable, the core is wrapped with 20 mil thick semi-conductive swelling tape, and in the case of the concentric neutral cable, the core is wrapped with 79 mil thick semiconductive swelling tape. The measured high frequency dielectric properties of these tapes are shown in Figure 23. As these tapes are highly compressible, the dielectric properties are likely to be a strong function of compression. For example in the case of the concentric neutral cable, the tape is compressed roughly 50% during manufacture.

Measured High Frequency Attenuation

Figure 24 shows the measured characteristic impedance and high frequency loss for the concentric neutral cable, and Figure 25 shows the characteristic impedance and loss for the cable with the corrugated Cu sheath.

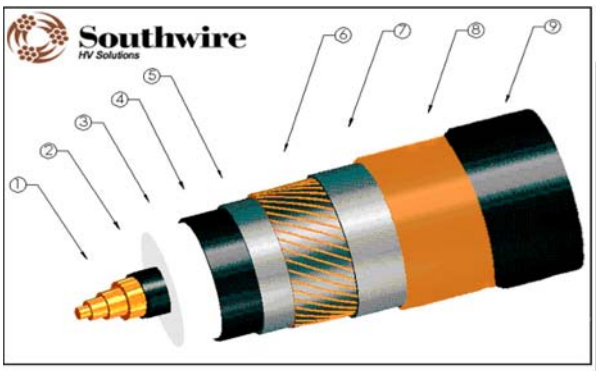

High Voltage Solid Dielectric Cable
69 kV — Copper conductor with Copper Laminate Sheath

Component	Description	Material	Thickness (mils)	Diameter (in.)
1	Reverse concentric stranded compressed Conductor 2000 kcmil — 127 strand	Copper	n / a	1.58
2	Conductor Shield	SC-XLPE	40	1.68
3	Super Clean XLPE Insulation	XLPE	450	2.58
4	Insulation Shield	SC-XLPE	70	2.72
5	Water-Swellable Semi-Conductive Tape	Polyester non-woven Fabric	79	2.87
6	Cu. Concentric Wires , 42 x 14 AWG	Copper	66	3.01
7	Water-Swellable Semi-Conductive Tape	Polyester non-woven Fabric	16	3.04
8	Laminated Sheath	Copper	6	3.05
9	Jacket	LLDPE	150	3.35
	Semi-Conductive Jacket Layer	SC-PE	10	3.37
Approximate Finished Cable Weight = 9.2 pounds per foot				

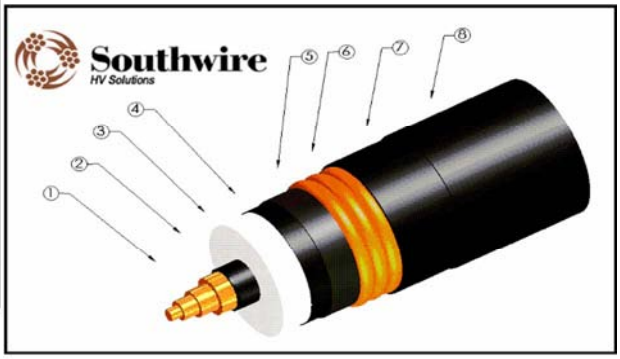

High Voltage Solid Dielectric Cable
69 kV — Copper conductor with corrugated Copper sheath

Component	Description	Material	Thickness (mils)	Diameter (in.)
1	Reverse concentric stranded compressed Conductor 2500 kcmil — 169 strand	Copper	n / a	1.77
2	Conductor Shield	SC-XLPE	40	1.86
3	Super Clean XLPE Insulation	XLPE	450	2.76
4	Insulation Shield	SC-XLPE	50	2.86
5	Water-Swellable Semi-Conductive Tape	Polyester non-woven Fabric	20	2.90
6	Welded and Corrugated Sheath	Copper	30	3.26
7	Jacket	LLDPE		
8	Semi-Conductive Jacket Layer	SC-PE		
Approximate Finished Cable Weight = 11.7 pounds per foot				

Figure 22. Construction of the two transmission class solid dielectric cables measured at the Southwire factory where they were manufactured. Figure courtesy of Southwire.

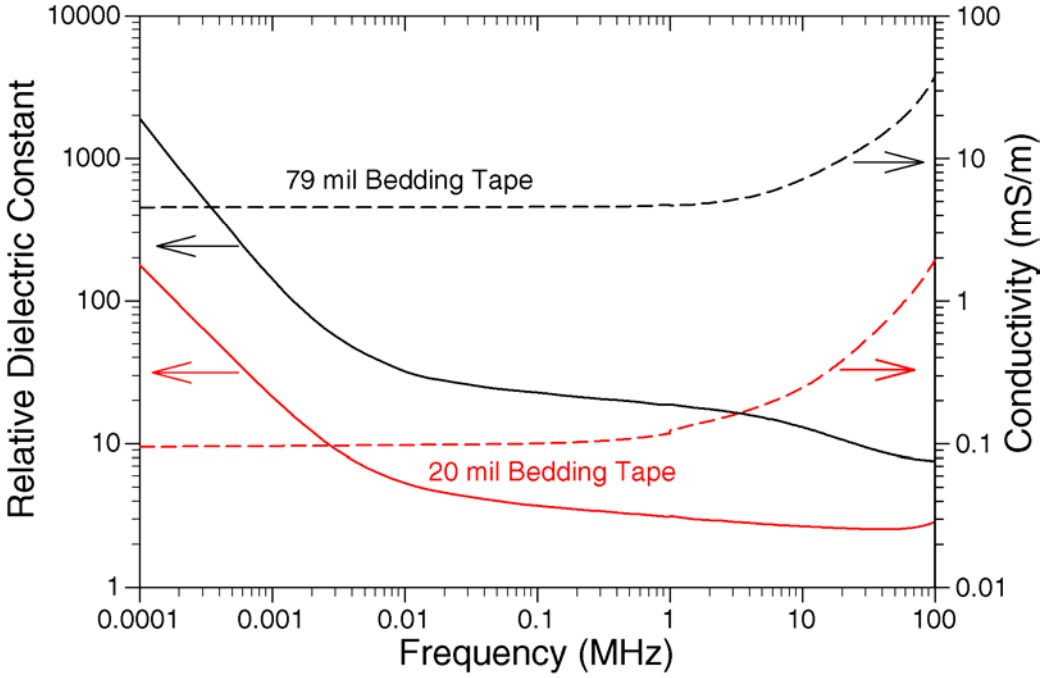

Figure 23. High frequency dielectric properties of the bedding layers used in the concentric neutral cable (79 mil) and Cu sheath cable (20 mil).

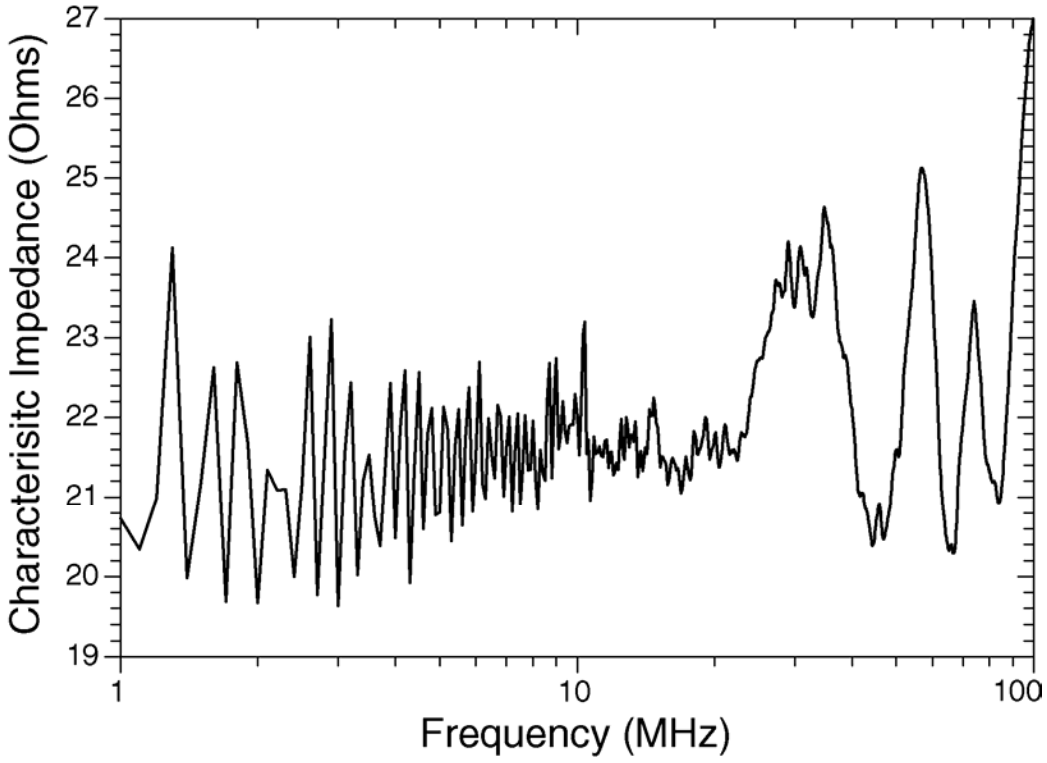

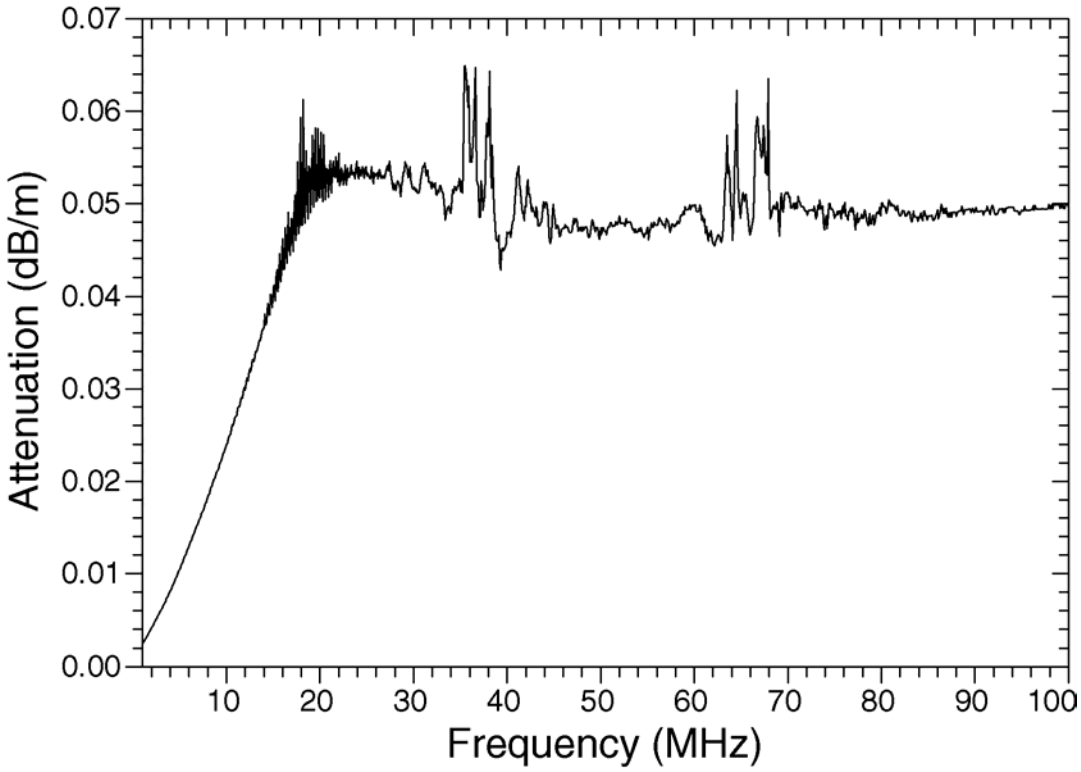

Figure 24. Characteristic impedance and high frequency attenuation measured for the transmission class concentric neutral cable. The measurement technique involves measuring the impedance as a function of frequency with the "far" end open circuit and short circuit. The characteristic impedance and attenuation are computed from these data. Periodic resonances in the measurements cause "noise" in the computed characteristic impedance and attenuation. However, the trend is clear.

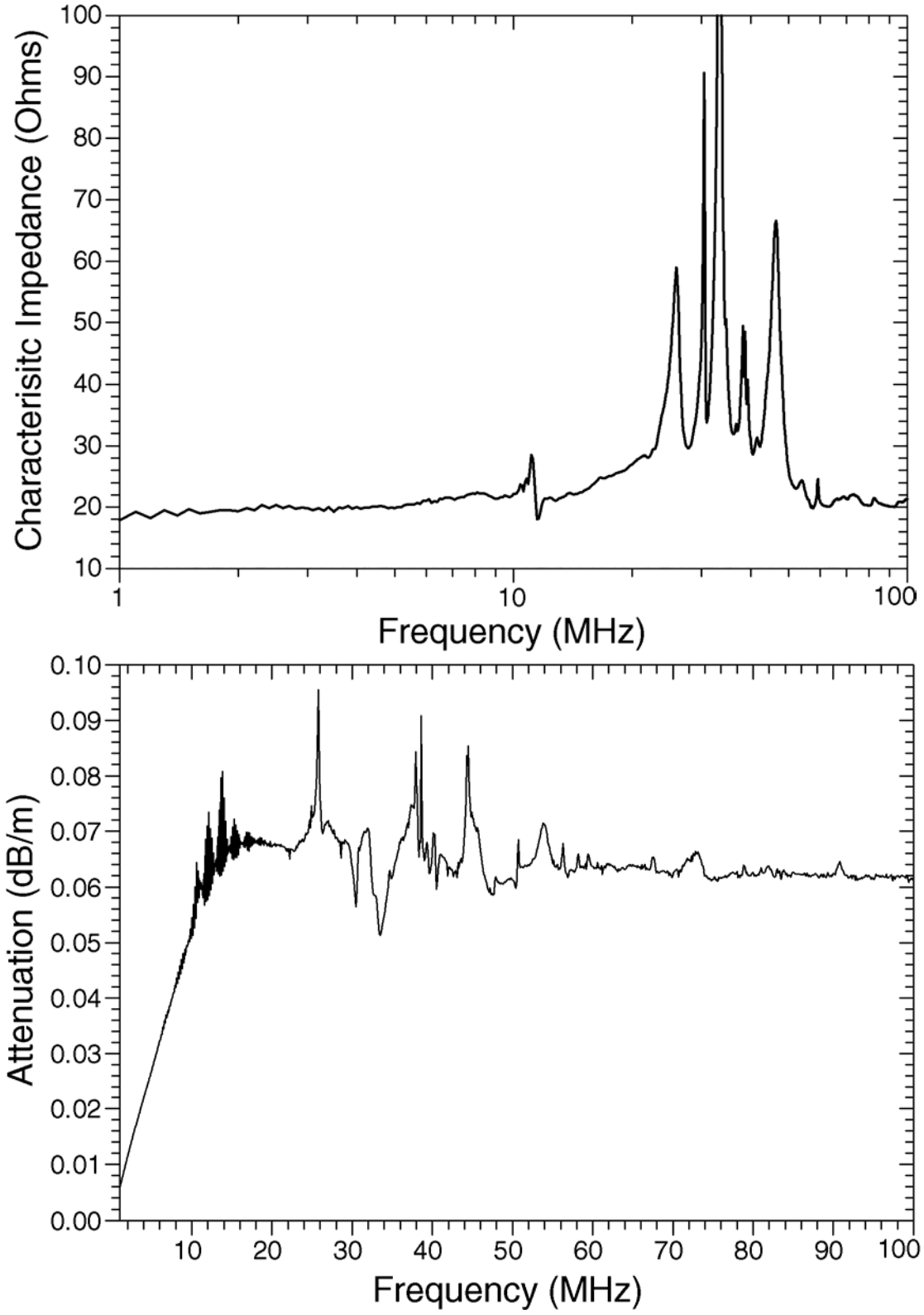

Figure 25. Characteristic impedance and attenuation as a function of frequency for the corrugated Cu sheath cable. Some strong resonances in the data are evident in the 20 to 50 MHz range, but the trends in characteristic impedance and attenuation are clear in spite of these resonances.

For both cables, the data show signs of resonances, which are inevitable in such measurements. The propagation characteristics are determined using a high frequency impedance analyzer to measure the impedance of the cable as a function of frequency first with the "far" end open circuit and then with the far end short circuit. The characteristic impedance and attenuation are then computed from

$$Z_c(f) = \sqrt{Z_{open}(f) \cdot Z_{short}(f)} \tag{25}$$

$$\gamma(f) = \frac{1}{L} \arctan\left(\sqrt{\frac{Z_{short}(f)}{Z_{open}(f)}} \right) \tag{26}$$

where L is the cable length and $Z_{open}(f)$ and $Z_{short}(f)$ are the impedance as a function of frequency measured from one end of the cable with the opposite end of the cable open circuit and short circuit, respectively. $\gamma(f)$, the attenuation constant, is in Nepers/m and can be converted to dB/m by multiplying by $20 \log_{10}(e) = 8.686$.

For both cables, the attenuation increases fairly linearly from 1 MHz to about 10 MHz in the case of the cable with the corrugated Cu shield and about 15 MHz in the case of the concentric neutral cable, after which the attenuation levels off, at about 0.05 dB/m in the case of the concentric neutral cable and about 0.06 dB/m in the case of the cable with the corrugated Cu sheath. This type of characteristic is fairly common in working with structures which have series elements. Normally the leveling of the high frequency attenuation is the result of having an element with a purely capacitive impedance (the dielectric) in series with one or more elements which have a complex impedance which can be modeled as a resistor in parallel with a capacitor. At low frequencies, the resistive impedance is lower than the capacitive impedance, so the current through the resistive impedance increases linearly with frequency, i.e., with the capacitive current through the dielectric, as the dielectric has a much greater impedance than the resistive layer (shield or bedding). At some frequency, the capacitive impedance of the RC layer become equal to the resistive impedance, and above that frequency, the RC layers increasingly forms a capacitive divider with the purely capacitive layer, which results in a constant voltage across the resistive component of the RC layer. This results in constant power loss in the resistive layer which translates to constant attenuation with frequency. Given the very high conductivity of the shields used in these cables, the relevant RC layer must be the bedding layer. This layer is designed to be "spongy" in order to take up thermal expansion of the XLPE while maintaining electrical continuity between the cable ground shield and the neutral wires or Cu sheath. Inevitably, this layer is compressed by the cable core and by the manufacturing process in the case of the concentric neutral cable. As a result, the high frequency properties of these layers are very difficult to predict. In the case of the Cu sheath cable, the cable core is somewhat loose in within the sheath at room temperature. As a result, the electrical resistance from the ground shield to the Cu sheath will be lower at the bottom of the cable, where the bedding layers are compressed, than at the top. This can result in some additional sources of high frequency loss, such as circumferential currents in the ground shield. As a result of all these considerations, predicting the loss of these cables from first principles is very difficult, even after measurement of the bedding layer dielectric properties, as those properties are a function of compression, and the degree of compression is either not known or is variable.

Implications of Measured High Frequency Attenuation

The measured high frequency attenuation is of a peculiar nature, although easily explained. The result of the essentially constant attenuation over most of the frequency range is that the PD pulse is attenuated with little change in its shape, although a broad peak develops under the sharp peak, caused by the linearly increasing attenuation at relatively low frequency. The sharp peak decreases in amplitude with distance propagated more rapidly than the broad peak, so at about 1000 m, the broad peak "swallows" the narrow peak. The solid lines in Figure 26 show the relative pulse amplitude as a function of distance propagated of the sharp pulse which rides on top of the broad pulse. The dashed lines show the total pulse magnitude, i.e., the absolute peak amplitude, which decreases less rapidly at large distance than the amplitude of the sharp peak.

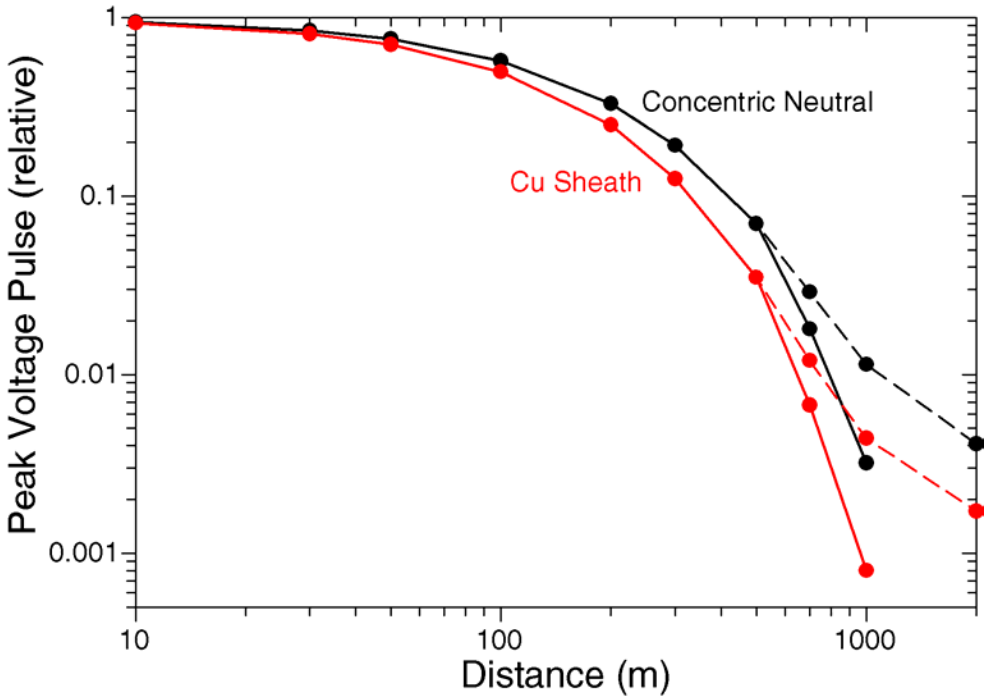

Figure 26. Relative PD pulse peak amplitude as a function of distance propagated down the concentric neutral and Cu sheath transmission class cables. The solid line shows the amplitude of the narrow pulse which is essentially the same shape as the initial PD pulse but which is sitting on top of a broad pulse decreases in amplitude less rapidly as a function of distance than the sharp peak. The dashed line shows the total amplitude. Beyond about 1000 m, the sharp pulse disappears, having been "swallowed up" by the broad pulse.

Figure 27 shows the relative peak PD pulse amplitude as a function of distance propagated for the PPLP, transmission class XLPE, and a distribution class TR-XLPE cable for comparison. As expected, the PPLP cable has the greatest pulse attenuation. At 1000 m, a PD pulse propagating down the PPLP cable is about an order of magnitude smaller than one propagating down the concentric neutral transmission class XLPE cable. Also at 1000 m, the transmission class XLPE cables have similar pulse attenuation to a TR-XLPE distribution cable.

As is clear from Table 1, high frequency attenuation can vary substantially even for cables of the same technology. This will also be true of transmission class solid dielectric cable, as a result of differences in the shield and bedding layers employed. The latter could vary in high frequency

dielectric constant or conductivity by orders of magnitude from those characterized in this report. In addition, the high frequency attenuation is likely to change with operating temperature as a result of compression of the bedding layers. Such compression should increase the conductivity of the bedding layers, which will probably reduce the high frequency loss, although this is not certain. Given the lack of data in the literature for the propagation characteristics of transmission class solid dielectric cable, the measurements presented here are certainly better than what was available previously, and they point toward high frequency attenuation characteristics which differ appreciably from distribution cable as a result of the relatively high resistivity bedding layers.

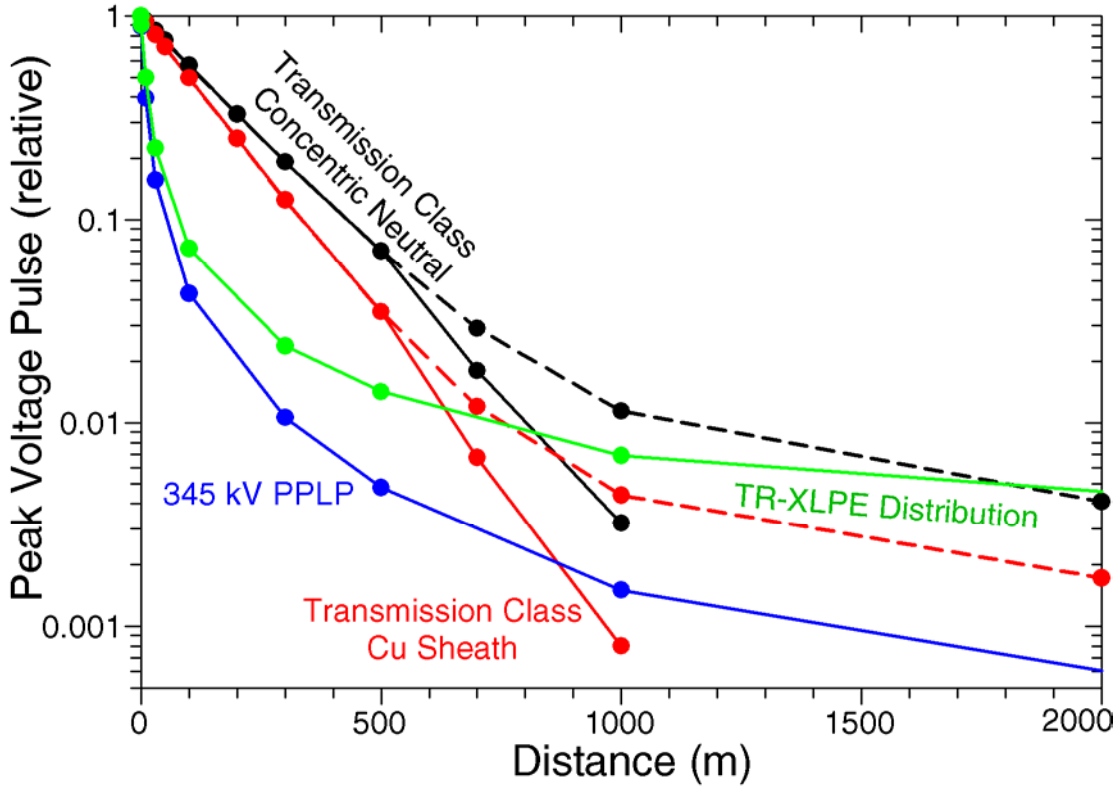

Figure 27. Relative PD peak pulse amplitude as a function of distance propagated for various cable technologies. As expected, the 345 kV PPLP cable has greater high frequency attenuation than other cables technologies. Out to 1000 m, the transmission class solid dielectric cable has a pulse attenuation which is less than, or at worst comparable to, TR-XLPE distribution cable.

Conclusions

The above data indicate that the transmission class XLPE cable has the interesting property of a much lower pulse attenuation than distribution cable to a distance of about 500 m, beyond which the attenuation is comparable to XLPE distribution cable. Obviously PPLP cable has much greater high frequency pulse attenuation than other technologies.

6

OPTIONS FOR IN-SERVICE PD MONITORING

Introduction

All of the approaches discussed in the literature review of Chapter 3 require an expert operator to achieve a sensitivity in the range of 10 pC over an entire cable installation and 1 pC near the PD couplers. The characteristics which will have to be exploited in order to develop an automated system with similar sensitivity are:

1. That very large amounts of time are available for automated detection.
2. That wideband, wide dynamic range IC A/D converters are now readily available. For example 14-bit A/D converters are available with a sampling rates of 190 MS/s (~80 MHz bandwidth) [1] and 13-bit A/D converters are available with sampling ranges in the range of 250 MS/s (~100 MHz bandwidth) [2].
3. Recent software developments in clustering PD (or noise) pulses from different sources, and then analyzing the pulses from each source to determine their cause.

The limitations which should be respected include:

1. No wideband communication should be required between PD detection nodes in the system. A need for all nodes to be connected by wideband links would probably increase system cost greatly. Thus PD analysis should be local or PD pulse characteristics should be reduced to a small number of parameters which can be communicated to a central processor over a narrow band link.
2. Each PD detection node in the system should have the ability to separate noise pulses from PD pulses, preferably without data from other nodes in the system.

PD Couplers

Based on the literature, the obvious approaches to PD couplers are metal electrodes installed on the ground shield semiconducting layer of a splice or the adjacent cable. This requires that splices be purchased with such couplers manufactured into the splice and that a connection to the sensing "patch" on the semicon be brought through the splice casing. Such penetrations are always a concern, as they tend to be a source of leaks. Alternatively, if a PD monitoring system must be retrofitted to an existing cable without such couplers, detecting PD as a voltage across insulating joints is an option, assuming that they are part of the design. Such joints will increase the background noise level as they allow electromagnetic noise to enter the cable system, whether the PD coupler is at the insulating joint or installed as part of splices. Couplers installed in joints do not have this disadvantage.

PD Signal Acquisition

Noise is always a major problem, especially as it limits the ability to trigger on a PD pulse above the threshold of continuous noise. One way to overcome this limitation is to digitize data continuously for several power frequency cycles and then search for PD pulses in the data using techniques such as wavelet transforms. This approach avoids the need to trigger on a PD pulse above the noise but is time consuming, as only a few cycles can be digitized at a time at the required sampling rate (at least twice the bandwidth), and the time required for wavelet analysis will be much greater than the time to acquire the data. Thus this approach has a low duty cycle and can be cumbersome when applied during field tests. In an automated monitoring system, these disadvantages are not important limitations, as the system can operate 24 hours a day, unattended. Also, the duration of continuous data which can be collected and stored will continue to increase as the price of memory continues to drop. The time required for computationally intensive analysis, such as wavelet analysis, will continue to decrease as microprocessors become more powerful. Thus in a continuous on-line monitoring situation, untriggered signal acquisition followed by sophisticated digital signal processing is probably the best option for PD signal acquisition.

Noise Rejection and Multiple PD Sources

As PD-like pulses (noise or PD) are collected, they must be clustered into different sources which can later be analyzed to determine if they are noise or PD, and if PD of what cause. Techimp [3,4] has developed a good basis for automated clustering of PD pulse data on the basis of pulse duration vs pulse bandwidth (Figure 27). Based on their work and commercial instruments, this tends to cluster PD pulses from various sources so that the pulses from each source can be analyzed separately, which is essential if PD is to be categorized when more than one source is present. In combination with untriggered data acquisition, this approach also allows PD sources of widely differing PD amplitude to be categorized simultaneously.

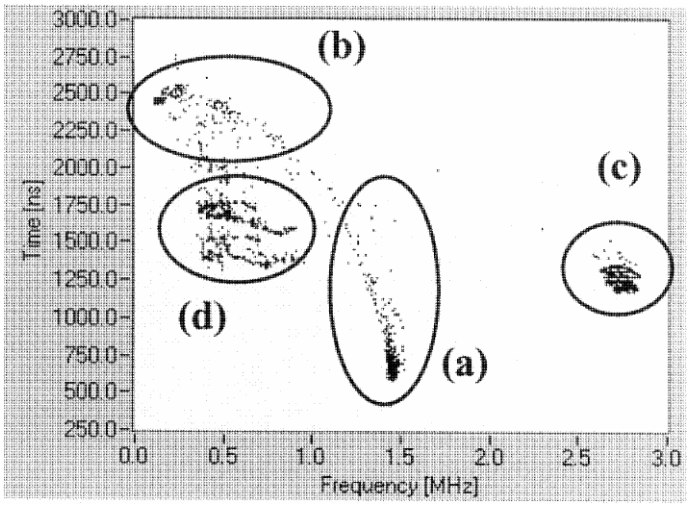

Figure 27. PD pulse cluster map from [3]. Four sources of PD-like pulses are present which can be analyzed separately to determine their nature. The analysis indicated that (a) is PD in a cable termination, (b) is scattered noise pulses, (c) are pulses which exceeded the dynamic range of the system, and (d) is rectifier noise in the variable frequency resonant test set.

PD Categorization

Finally, the PD pulse clusters, as seen in Figure 27, must be analyzed to determine their nature. Figure 28 shows the analysis of two of the clusters in Figure 27 [3]. Again, Techimp has advanced the art through automated analysis based on both Weibull pulse height [5], pulse height vs phase, and the distribution of time between PD pulses [6]. These approaches combined with "fuzzy logic" algorithms to identify PD sources as surface (interfacial) discharges, corona, cavity discharges, noise, or invalid data. A probability is assigned to each cause of the pulse cluster as identified above. This technology, which has been applied to cable [3], appears to facilitate automated PD analysis as would be necessary for an on-line monitoring system in order to avoid false positives from noise.

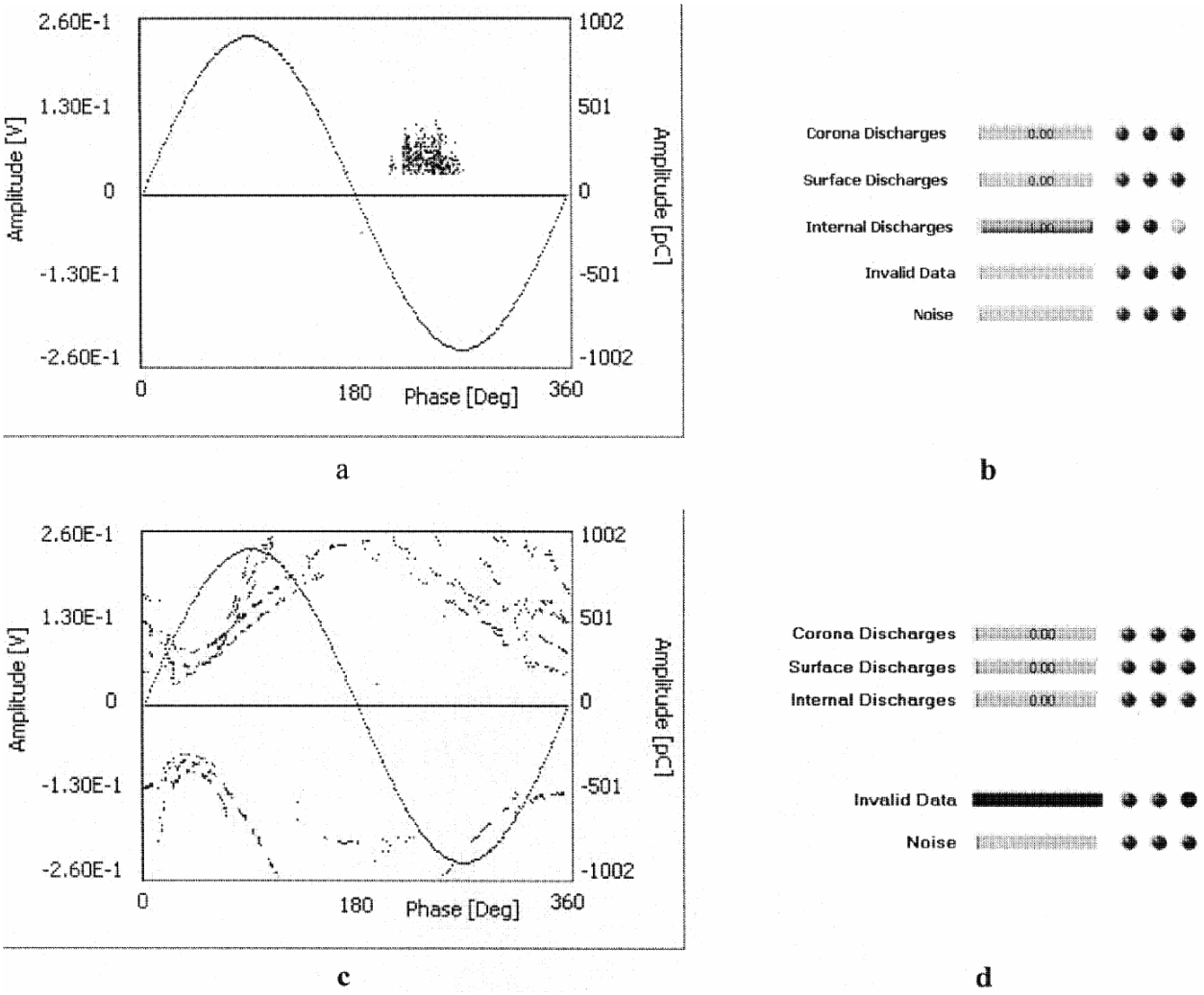

Figure 28. Identification of two of the PD clusters of Figure 27 [3]. (a) shows the phase resolved PD pattern of cluster (a) in Figure 27, which, as shown in (b), is identified with 100% certainty as "Internal Discharges", in this case within a cable termination. (c) shows the phase resolved PD pattern of cluster (b) in Figure 26, which is identified as "Invalid Data" with 100% certainty .

Communications

The above technology could reduce the information which must be transmitted to an alarm and diagnosis, or it could transmit only the data upon which the diagnosis was based. In either case, the amount of information which must be transmitted from each terminal is infrequent and small. Based on a previous EPRI project, this information could probably be transmitted on the cable sheath or ground structure, if necessary.

Expected Sensitivity

Based on the measured attenuation properties of the transmission class XLPE cable and assuming untriggered PD signal acquisition with state-of-the-art DSP followed by PD source clustering and identification as discussed above, a sensitivity in the range of 10 pC for maximum distance to the PD source of 1000 m seems reasonable, assuming the low background noise levels which you would expect for a hermetic system with a continuous or nearly continuous conducting sheath. This is consistent with Figure 13, if one assumes the matched filter response with a required S/N ratio in the range of 3 dB rather than the 10 dB assumed in Figure 13, which would imply a factor of ~2 improvement in sensitivity. Thus with a fixed 20 MHz bandwidth, the sensitivity would be about 5 pC close to the PD source and about 10 pC at 1000 m. Of course the noise level in a transmission class XLPE cable is likely to be less than the 1 $\mu V/\sqrt{Hz}$ assume, and the PD detection sensitivity varies as the square of the noise spectral density, so that halving the spectral density to 0.5 $\mu V/\sqrt{Hz}$ would improve the PD detection sensitivity by a factor of 4, to the range of 1 pC near the PD source and 2 pC far from the source. The small change with distance is the result of using a much less than optimum bandwidth, which limits the sensitivity for PD sources close to the coupler. For a 20 Ω transmission line, the thermal noise is about 0.6 $nV/\sqrt{Hz}$, so even at 0.5 $\mu V/\sqrt{Hz}$ we are assuming a noise spectral density which is a factor of 1000 greater than the fundamental thermal noise of a 20 Ω source.

The optimum PD detection bandwidth for such a system requires some study. The important considerations include:

- As the bandwidth and required sampling rate increase, the duration of data which can be acquired and stored with a given memory decreases, resulting in a lower duty cycle for the system.
- As the sampling rate increases, resulting in more data per unit time, the DSP processing of the time will increase, again reducing the duty cycle of the system.
- Increased PD detection bandwidth will improve PD detection sensitivity for PD sources very close to the PD coupler but will have no positive impact for other PD sources.

Thus the primary reason for increasing the PD detection bandwidth would be to improve PD sensitivity at the splices on which the PD couplers are most likely to be installed, and this could be a good reason to employ a bandwidth in the 100 MHz range. One possibility would be to use the full bandwidth in looking for PD in splices but then process the data to reduce the bandwidth before looking for PD sources in the cable.

Conclusion

The Techimp PD clustering and identification technology appears to provide the best available basis for development of an automated PD monitoring system for transmission class cables. As well, their technology has been fairly well documented in the literature. An automated PD monitoring system appears to be practical based on a combination of state of the art wideband, wide dynamic range A/D converters, large solid state memories which allow several cycles of data to be digitized with a bandwidth of 20 MHz or more, DSP denoising of the acquired data, and PD pulse clustering and identification technology,

Based on the information in the literature and on measurements carried out during this project, a sensitivity in the range of 10 pC can be expected over the full extent of a transmission cable system assuming that PD couplers are located no more than 1000 m apart.

References

1. Texas Instruments web site: http://focus.ti.com/docs/prod/folders/print/ads5546.html
2. Texas Instruments web site: http://focus.ti.com/docs/prod/folders/print/ads5444.html
3. A. Cavallini, A. Contin, G.C. Montanari, and F. Puletti. "Advanced PD Inference in On-Field Measurements. Part I: Noise Rejection". IEEE Trans DEI-10, No. 2, April 2003. pp. 216-224.
4. A. Contin, G.C. Montanari, and C. Ferrano. "PD Source Recognition by Weibull Processing of Pulse Height Distributions". IEEE Trans DEI-7, No. 1, Feb. 2000. pp. 48-58.
5. A. Cavallini, M. Conti, A. Contin, and G.C. Montanari. "Advanced PD Inference in On-Field Measurements. Part II: Identification of Defects in Solid Insulation Systems". IEEE Trans DEI-10, No. 3, June 2003. pp. 528-537.
6. A. Cavallini, F. Puletti, and A. Contin. "A New Methodology for the Identification of PD in Electrical Apparatus: Properties and Applications". IEEE Trans DEI-12, No. 2, April 2005. pp. 203-215.

Export Control Restrictions

Access to and use of EPRI Intellectual Property is granted with the specific understanding and requirement that responsibility for ensuring full compliance with all applicable U.S. and foreign export laws and regulations is being undertaken by you and your company. This includes an obligation to ensure that any individual receiving access hereunder who is not a U.S. citizen or permanent U.S. resident is permitted access under applicable U.S. and foreign export laws and regulations. In the event you are uncertain whether you or your company may lawfully obtain access to this EPRI Intellectual Property, you acknowledge that it is your obligation to consult with your company's legal counsel to determine whether this access is lawful. Although EPRI may make available on a case-by-case basis an informal assessment of the applicable U.S. export classification for specific EPRI Intellectual Property, you and your company acknowledge that this assessment is solely for informational purposes and not for reliance purposes. You and your company acknowledge that it is still the obligation of you and your company to make your own assessment of the applicable U.S. export classification and ensure compliance accordingly. You and your company understand and acknowledge your obligations to make a prompt report to EPRI and the appropriate authorities regarding any access to or use of EPRI Intellectual Property hereunder that may be in violation of applicable U.S. or foreign export laws or regulations.

The Electric Power Research Institute (EPRI)

The Electric Power Research Institute (EPRI), with major locations in Palo Alto, California, and Charlotte, North Carolina, was established in 1973 as an independent, nonprofit center for public interest energy and environmental research. EPRI brings together members, participants, the Institute's scientists and engineers, and other leading experts to work collaboratively on solutions to the challenges of electric power. These solutions span nearly every area of electricity generation, delivery, and use, including health, safety, and environment. EPRI's members represent over 90% of the electricity generated in the United States. International participation represents nearly 15% of EPRI's total research, development, and demonstration program.

Together…Shaping the Future of Electricity

Printed on recycled paper in the United States of America

1012338

Electric Power Research Institute
3420 Hillview Avenue, Palo Alto, California 94304-1338 • PO Box 10412, Palo Alto, California 94303-0813 • USA
800.313.3774 • 650.855.2121 • askepri@epri.com • www.epri.com